

Final Report

Project Title Prevent Solidification Defects for Large Superalloy Castings Used in Advanced Electric Power Systems

Covering Period: September 2005 to August 2007

Date of Report: September 2007

Recipient Organization: West Virginia University Research Corporation
On behalf of West Virginia University
886 Chestnut Ridge Road
P.O. Box 6845
Morgantown, WV 26506

Award Number: DE-FC36-03G013026

Subcontractor: Pennsylvania State University
Zi-Kui Liu
(814) 865-1934
zikui@psu.edu

Industrial Partners: Special Metals Corps
John J. deBarbadillo
(304) 526-5634
jdebarba@specialmetals.com

GE Energy
Joseph J. Jackson
(864) 254-4332
JosephJ.Jackson@ps.ge.com

Technical Contact: Xingbo Liu
West Virginia University
(304) 293-3111 x. 2324
Xingbo.liu@mail.wvu.edu

Business Contact: Alan Martin (WVU Business Officer)
(304) 293-3998
Alan.Martin@mail.wvu.edu

DOE Project Officer: Michelle New
National Association of State Energy Officials
(703) 299-8800
mnew@naseo.org

Project Objectives:

The objective of this project is to develop improved methodologies for preventing macrosegregation in superalloy remelting processes. A combination of theoretical modeling and physical experimentation will be used to address weaknesses in existing models, particularly the inability to accurately predict the partition of key elements between the liquid and solid phases during solidification. The ultimate goal is to develop a predictive technology that can be applied commercially to prevent solidification defects in large superalloy castings used in advanced electric power systems.

Background:

The rapidly growing need for clean, reliable, and affordable power across the United States has resulted in great demand for high-efficiency gas turbine power systems. To improve energy efficiency, reduce operating cost, and lower CO₂ emissions, gas turbines are operated at high temperature because the overall energy conversion efficiency depends on the firing temperature. Each 50°F increase in firing temperature results in a 1% increase in combined-cycle efficiency. Temperature limits of gas turbine operation are generally determined by the capability of the materials used for components such as turbine wheels and buckets to withstand the severe stresses associated with high-speed operation at high temperatures. Gas turbine components used in power generation are much larger compared to their aircraft counterparts (5 to 100 times heavier), and the slower cooling rate of the larger ingots during solidification dramatically increases the inhomogeneity of the chemical composition in the final product, leading to the formation of macrosegregation defects such as freckle (black spots rich in low melting-point compounds) and center segregation.

WVU, Penn State University (PSU), SMC, and GE Energy (GE) propose to study macrosegregation in superalloy remelting processes. Weaknesses in existing models, particularly the inability to accurately predict partition coefficients of key elements under real operating conditions, will be addressed. Compositional effects of individual alloying elements in different alloys will be characterized so that a comprehensive database will be available in a usable format. A predictive methodology incorporating advanced computation technologies will be developed. Alloy index of freckle and center segregation formation can be determined for complex alloy compositions with efficient computational and laboratory analysis. The ultimate goal is to develop a predictive technology that can be applied commercially to prevent solidification defects for large superalloy castings used in advanced electric power systems.

Accomplishment Summary:

The partition coefficients of the most important minor and major solute elements of model Ni-based alloys were studied by theoretical simulations and by physical experimentation. Standard instruments were used for the experiments and a methodology of production of laboratory size alloys was proposed, developed and refined. From the theoretical point of view, a better description of the Fe-Ni-Nb system was obtained with respect to the commercial database. Also, the influence of the method of calculation and the database used over the partition coefficients was addressed. In general, the experiments showed agreement with the theoretical calculations in the influence of the solute elements on the solidification characteristics, although some systematic variation of the experimental data was detected and requires further analysis. The Nb partition coefficient determined experimentally differed from the predicted by the commercial database. The experimental setup for directional solidification experiments was completed and an experimental plan was proposed to perform verification experiments on model and

commercial alloys, and evaluate the influence of the processing parameters on the macrosegregation defects. The results of the directional solidification experiments will be valuable in the formulation of a criterion for VAR freckling. A satisfactory interaction between research groups from WVU, PSU and NETL with Industrial partners was developed, opening new opportunities to work in future research projects.

Patents:

N/A

Publications/Presentations:

1. J. Valdes, X. B. Liu, S. L. Shang and Z. K. Liu, "Partition behavior of Nb in the Ni-Cr-Fe-Nb alloy system", 18th AeroMat Conference and Exhibition, June 25-28, 2007, Baltimore, Maryland (oral presentation).
2. J. Valdes, S. L. Shang, Z. K. Liu, X. B. Liu and P. King, "Investigation of the partition coefficients in the Ni-Cr-Fe-Nb alloys", Superalloys 2008, Sept. 14-18, 2008, Champion, Pennsylvania (presentation, to be attended).
3. S. L. Shang, Y. Wang, D. E. Kim and Z. K. Liu, "Coefficients of thermal expansions of the γ and γ' phases in Ni-based superalloys: an *ab initio* phonon approach", Superalloys 2008, Sept. 14-18, 2008, Champion, Pennsylvania (presentation, to be attended).
4. D. E. Kim, S. L. Shang, X. B. Liu and Z. K. Liu, "Thermodynamic modeling of the Ni-Fe-Nb ternary system", Superalloys 2008, Sept. 14-18, 2008, Champion, Pennsylvania (presentation, to be attended).
5. S. L. Shang, J. Valdes, D. E. Kim, X. B. Liu and Z. K. Liu, "Partition behaviors of alloying elements in the Ni-Cr-Nb alloys: thermodynamic and kinetic investigations", Materials Science and Engineering A (to be submitted in 2007).
6. D. E. Kim, S. L. Shang, J. Valdes, X. B. Liu and Z. K. Liu, "Thermodynamics of the Fe-Nb-Ni system: application for the prediction of partition coefficients" (in preparation).
7. D.E. Kim, S.L. Shang, X. B. Liu, and Z. K. Liu, "Thermodynamic modeling of the Cr-Fe-Nb system" (in plan).

Task 1: Solidification Modeling

Task 1.1 Thermodynamics Database and Partition Coefficients

Sub-task 1.1.1 Thermodynamic Modeling (Liu/PSU)

The goal for this subtask is to perform theoretical investigation of partition coefficients in Ni-based superalloys through first-principle calculation and thermodynamic/kinetic modeling. To this end, the ternary and quaternary model alloys in the Ni-Cr-Fe-Nb system are selected in the present work. During the last two years, the research efforts were focused on studying:

- (i) the valid thermodynamic descriptions in the Ni-Cr-Fe-Nb system,
- (ii) the thermodynamic modeling of the ternary Ni-Fe-Nb system,
- (iii) the methods to predict partition coefficients of alloying elements,
- (iv) the effects of different thermodynamic database on the predicted partition coefficients,
- (v) the partition coefficients of Cr and Nb in the Ni-Cr-Nb alloys,
- (vi) the partition coefficients of Fe and Nb in the Ni-Fe-Nb alloys,
- (vii) the partition coefficients of interstitial element C in the Ni-C-Cr-Nb alloys,
- (viii) the build of ternary special quasirandom structures (SQSs) to be used in the first-principles calculations for disordered alloys.

(i) Thermodynamic descriptions in the Ni-Cr-Fe-Nb system

The valid thermodynamics of the Ni-Cr-Fe-Nb system is a fundament to predict the partition coefficients in the Ni-Fe base superalloy. Therefore it is worth to go in details to investigate the available commercial Ni-database and the recent progresses in this system. In the Ni-Cr-Fe-Nb system, four ternary systems are included, of which only the Cr-Nb-Ni and Cr-Fe-Ni systems have been modeled in the Ni-database. For the Cr-Nb-Ni system, the recent modeling work was done by Du et al [1]. For the Cr-Fe-Ni system, the recent modeling work was done by Tomiska [2]. However, for both the Fe-Nb-Ni and Cr-Fe-Nb systems, the ternary interactions are absent in the Ni-database and also the literature. For the Fe-Nb-Ni system, the recent investigation [3] indicates that a compound with hexagonal structure was observed at composition around Ni-20Fe-22Nb (at.%), but the further information is scarce about this unknown phase, e.g., the detailed crystal structure, the melting point, and the formation enthalpy etc. The existence of this unknown phase makes the modeling of Fe-Nb-Ni system difficult. Even for the binary Fe-Ni system, the current modeling do not describe well the γ' phase (FeNi_3) due to the existence of magnetism [4]. For the Cr-Fe-Nb system, no ternary compounds were reported in the literature [5].

In summary, the Ni-database needs to be improved by the recently modeled Cr-Nb-Ni and Cr-Fe-Ni systems, and the ternaries Fe-Nb-Ni and Cr-Fe-Nb are needed to be modeled in order to get a better thermodynamic description of the Cr-Fe-Nb-Ni system.

(ii) Thermodynamic modeling of the Ni-Fe-Nb system

The Ni-Fe-Nb system has been improved comparing with the Ni-Fe-Nb system in the commercial database in following features:

1. the Ni-Fe system is remodeled in order to describe well the γ' (FeNi_3) phase;
2. the μ phases in the Fe-Nb binary system and the Fe-Ni-Nb ternary system are remodeled correctly by using the four-sublattice model, while the three-sublattice model is

adopted by the commercial database, which can not give the correct site occupations of Nb;

3. the predicted phase boundaries of the all phase regions especially δ -Ni₃Nb and Laves phases in the Ni-Fe-Nb system are in good agreement with the measurements at 1473 K;
4. the predicted phase boundaries in the Ni-Fe-Nb system at 1273 K show better agreement with the isothermal sections of the Ni-Co-Nb and Co-Fe-Nb systems.

(ii-1) Thermodynamic modeling of the Fe-Ni system

The thermodynamic modeling of the Fe-Ni system in the commercial Ni-database does not describe well the γ' (FeNi₃) phase due to the existence of magnetism. We therefore re-modeled the ordered γ' phase using a three-sublattice model,



where Va represents the vacancy. The parameters in the Gibbs energy expression for the above three-sublattice model were estimated by the PARROT module in the Thermo-Calc code.

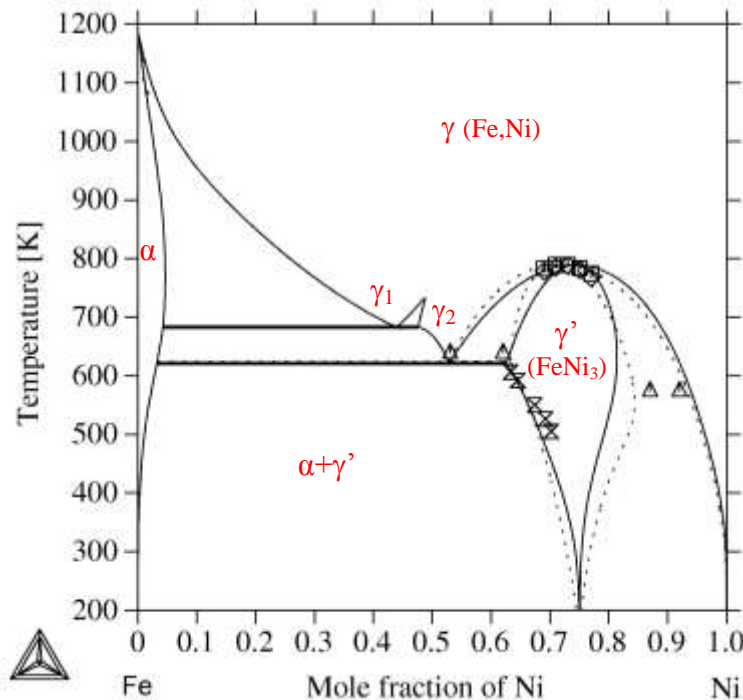


Fig. 1. Fe-Ni phase diagram calculated by present work (solid lines) and the commercial Ni-database (dotted lines). The symbols show the measured phase boundaries.

The obtained Fe-Ni phase diagram is shown in Fig. 1, where the symbol α represents the BCC disordered phase, γ the disordered FCC phase, γ' the ordered phase, i.e., FeNi₃. γ_1 and γ_2 represent the non-magnetic and magnetic disordered FCC phases, respectively. Fig. 1 shows that the presently calculated phase boundaries agree well with the measured ones. The modeled Fe-Ni system provided a starting point for the investigation of Ni-Fe-Nb system.

(ii-2) Thermodynamic modeling of the Fe-Nb system

The three-sublattice model, $(\text{Fe,Ni})_6 : (\text{Nb})_4 : (\text{Fe,Nb,Ni})_3$, is used in the commercial database [6] but it can not describe the site occupation of Nb correctly. Basically, there are 5 kinds of equivalent atomic positions in the μ phase: 1a, 2c1, 2c2, 2c3, and 6h with coordination numbers of 12, 15, 14, 16 and 12, respectively. The Nb occupancies of each site were measured by Joubert and Feutelais [7] and the results are given in Table 1 [8].

Table 1. Nb occupancies on the 5 sites of μ phase in the Ni-Nb system (at. %)

μ phase composition	Nb occupancy 1a	Nb occupancy 3c ₁	Nb occupancy 3c ₂	Nb occupancy 3c ₃	Nb occupancy 6h
Nb _{53.4} Ni _{46.6}	84%	94%	100%	78%	10%
Nb _{55.3} Ni _{44.7}	81%	99%	100%	85%	12%
Nb _{56.9} Ni _{43.1}	81%	100%	100%	81%	16%

As we can see in Table 1, the 3c₁ and 3c₂ sites are almost filled with Nb atoms and the other sites, 1a, 3c₃ and 6h, are partially filled with Nb atoms. 3c₁ and 3c₂ sites, therefore, can be considered as the same sublattice while the other sites take different sublattices. As a result, the four-sublattice model, $(\text{Ni,Nb})_1 : (\text{Nb})_4 : (\text{Ni,Nb})_2 : (\text{Ni,Nb})_6$, was adapted in the Ni-Nb system [9] as a description for the μ phase. With this description, it is assumed that the sublattice model for the μ phase in the Fe-Nb binary system is the same as that in the Ni-Nb system in order to assess the Ni-Fe-Nb ternary system. In the recent Fe-Nb system assessed by Toffolon [10], the different four-sublattice model, $(\text{Fe,Nb})_1 : (\text{Nb})_4 : (\text{Fe,Nb})_2 : (\text{Fe})_6$, was used but it indicated that there is no Nb occupancy in the 6h site. The μ phase is therefore re-modeled so that the 6h site can have Nb atoms.

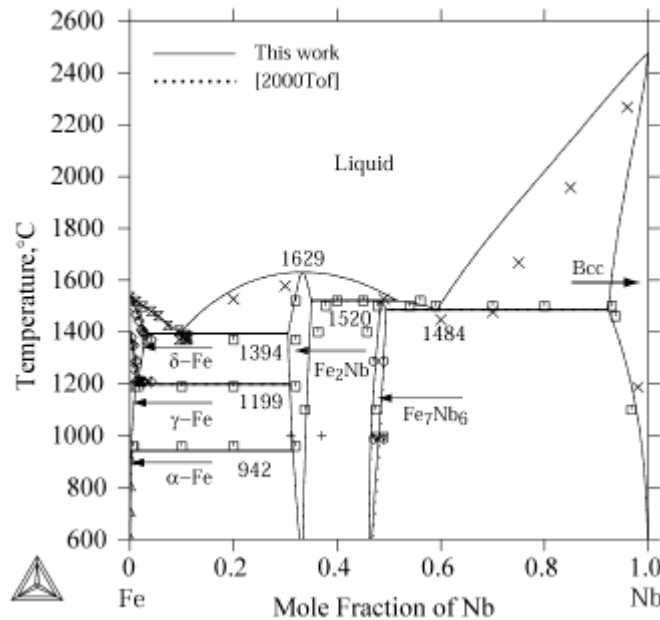


Fig. 2. Phase diagrams of the Fe-Nb system in this work (solid line) and by Toffolon[10](dotted line)

The phase diagram of the Fe-Nb system by using the new four-sublattice model, $(\text{Fe,Nb})_1 : (\text{Nb})_4 : (\text{Fe,Nb})_2 : (\text{Fe,Nb})_6$, is shown in Fig. 2 comparing with the work by Toffolon [10]. The phase boundary of the μ phase in the new Fe-Nb system is in good agreement with experimental data and the previous work by Toffolon [10]. Finally, the μ phase in the ternary system was described like following: $(\text{Fe,Nb,Ni})_1 : (\text{Nb})_4 : (\text{Fe,Nb,Ni})_2 : (\text{Fe,Nb,Ni})_6$. This

description of the μ phase is better than that of the commercial database in terms of the site occupancy of Nb because the three-sublattice model in the commercial database does not allow Nb atom to fill the 6h site at all unlike the experimental data of the Ni-Nb system.

(ii-3) Thermodynamic modeling of the Ni-Fe-Nb system

Based on the three binary systems, Fe-Ni (this work), Ni-Nb [9], and Fe-Nb (this work), the new Ni-Fe-Nb ternary system has been developed. There are few experimental data for the Ni-Fe-Nb ternary alloys, but an EPMA analysis of the ternary alloys at 1473 K was performed by Takeyama [11]. The ternary interaction parameters for the liquid phase are assessed in the present work in order to reproduce the experimental data on the isothermal sections. The calculated isothermal sections at 1473K of the Ni-Fe-Nb system by current work and by the commercial database are shown in Fig. 3 in comparison with experimental data [11].

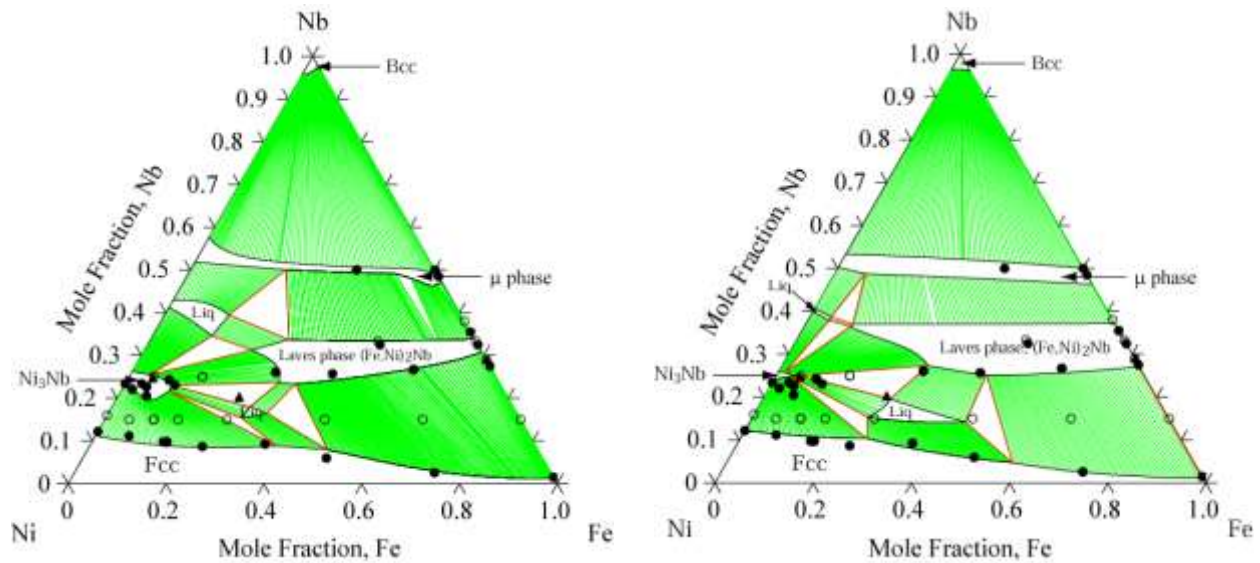


Fig. 3. Calculated isothermal sections at 1473K of the Ni-Fe-Nb system by the present work (left) and the commercial database (right) together with the experiments (●: phase boundary, ○: composition of bulk alloy, ▲: single phase)

The open circles and closed circles indicate the bulk alloy composition and phase boundary data, respectively. Each open circle should be in the 2-phase regions, but some open circles in the isothermal section of the commercial database are in the 3-phase regions (red triangle). The phase boundaries of the μ , Laves, and δ -Ni₃Nb phases in the new ternary system have also in better agreement with experimental data than those in the commercial database. Especially, the predicted solidus between FCC and δ -Ni₃Nb phases agrees well with the measurements at 1473K.

There is no direct ternary experimental data of this system at 1273K but Savin[12] reported some data about phase composition of the Ni-Fe-Nb alloys, which were estimated using the (s+d)-EC parameters of the Ni-Co-Nb or Co-Fe-Nb systems. These data are not reliable as the measurements. These, however, are the only experimental data except 1473K and can be used

to compare diagrams using these points. The calculated isothermal sections at 1273K of the new Ni-Fe-Nb system and of the commercial database are shown in Fig. 4.

In Fig. 4, the open symbols indicate single phase regions (circle-Ni₃Nb phase, triangle-Laves phase and square-μ phase) and closed circles mean 2-phase regions and closed triangle represent 3-phase regions. It should be mentioned again that the symbols are not experimental data and they do not indicate phase boundaries. Nevertheless Fig. 3 shows that the calculated isothermal section at 1273K of the new Ni-Fe-Nb system have better description for δ-Ni₃Nb phase than that of the commercial database.

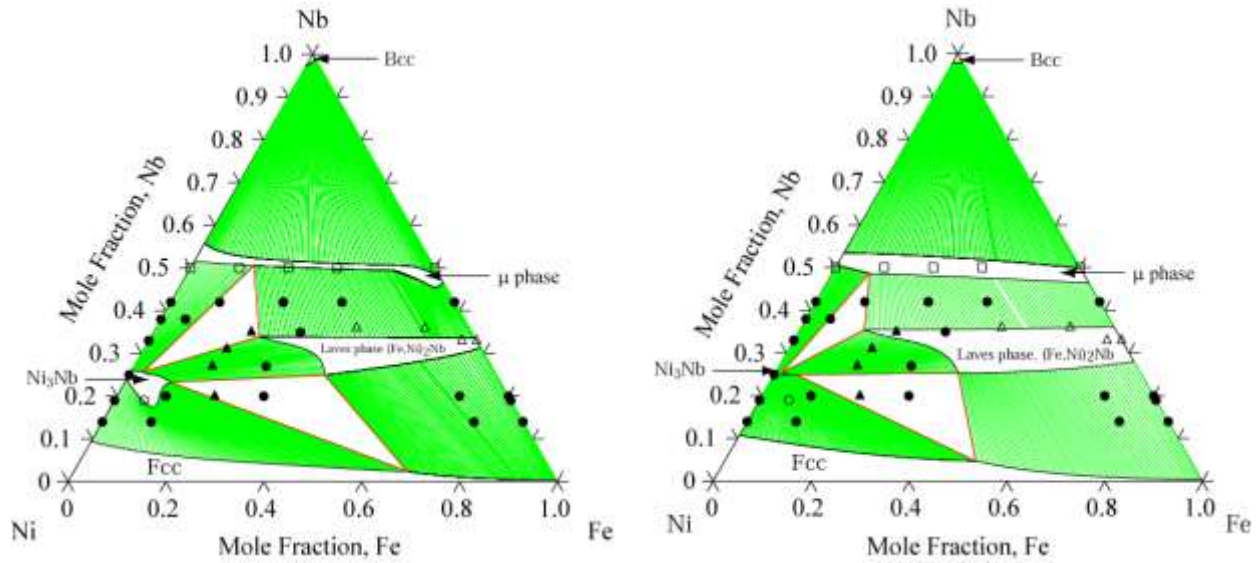


Fig. 4. Calculated isothermal sections at 1273K of the new Ni-Fe-Nb system(left) and of the commercial database(right) with the estimated values (○ : Ni₃Nb, △ : Laves, □ : μ phase, ● : 2-phases region, ▲ : 3-phases region)

(iii) Methods to predict partition coefficients of alloying elements

By considering the influences thermodynamics and kinetics, the methods to predict partition coefficients of alloying elements can be depicted by the following three,

1. Equilibrium calculation via the lever rule, i.e., at each temperature both solid and liquid phases are in thermodynamic equilibria, i.e. the diffusions of alloying elements in the liquid and solid phases are assumed to be infinitely fast;
2. Scheil's model: there are infinitely fast diffusions of all alloying elements in the liquid phase but no diffusions in the solid.
3. Back diffusion model (simulated by Dictra software), where the diffusions of alloying elements in the solid phase (the so-called back diffusions) and the liquid phase are not infinitely fast;

In the present work, the Thermo-Calc and Dictra software [13] are used to study the above methods (1), (2) and method (3), respectively. A model alloy Ni-15Cr-4.5Nb (in weight percent) is chosen to assess the effects of different simulation methods on the partition coefficients of Cr

and Nb. The used thermodynamic data are taken from the recent assessment [1], the used kinetic data are taken from the NIST mobility database [14].

During the simulation, only the liquid and solid (fcc) phases in Ni-15Cr-xNb alloys are considered. For the diffusion controlled phase transformation simulated by Dictra, the cooling rate 1 K/s is employed. The calculated solid fraction of Ni-15Cr-4.5Nb as a function of temperature is shown in Fig. 5. The predicted partition coefficients of Cr and Nb in Ni-15Cr-4.5Nb as a function of solid fraction are illustrated in Fig. 6. For solid fraction less than 0.5, Figs. 5 and 6 show that there are no obvious differences among the predicted properties by the three kinds of simulations: equilibrium calculation, Scheil model and back diffusion model. The considerable differences among the three kinds of simulations appear when solid fraction greater than 0.5. The back diffusion (Dictra) results (cooling rate 1 K/s) are located in the middle of the results obtained by equilibrium calculation and Scheil model, and close to those of the Scheil model. It is believed that the realized solidification is between the two extreme conditions: one is the complete diffusion in solid (equilibrium solidification), the other one is no diffusion in solid (Scheil model). Therefore the results from the Dictra simulation should be close to the realized condition. Fig. 5 shows that the solid plus liquid region is only 30 K for Ni-15Cr-4.5Nb under equilibrium condition, while the Dictra simulation, especially the Scheil model, predicts that the solidification takes place in a temperature range over 100 K. Fig. 6 shows that the partition coefficients of Cr and Nb increase with increasing of solid fraction. When solid fraction is greater than 0.8, both Dictra and Scheil simulations indicate that the increasing of partition coefficient of Nb is much faster than that of Cr. When the solid fraction is closer to 1, the partition coefficient of Cr shows a decreasing trend predicted both by Dictra simulation and Scheil model. Fig. 6 also indicates that the partition coefficient of Nb depends greatly on the solidification conditions, such as the cooling rate, when the solid fraction is close to 1.

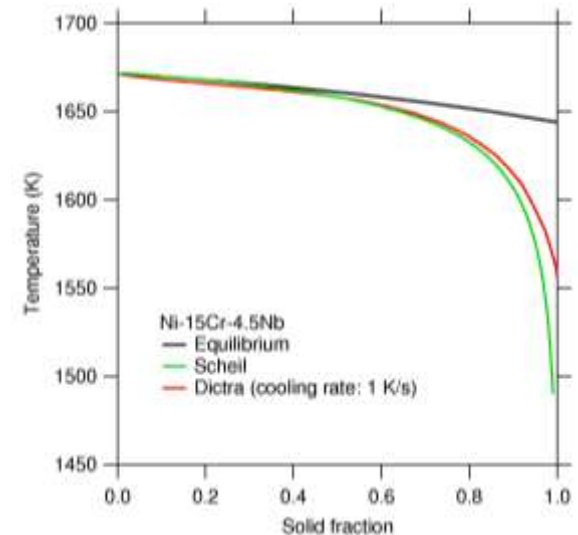


Fig. 5. Solid fraction of Ni-15Cr-4.5Nb as a function of temperature predicted by three different methods.

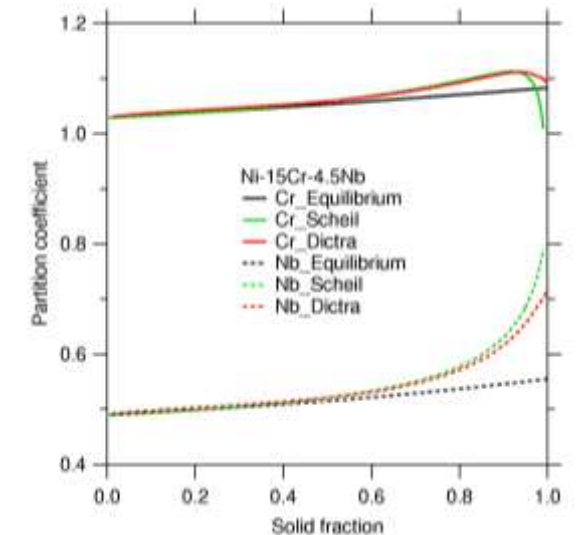


Fig. 6. Partition coefficients of Cr and Nb in Ni-15Cr-4.5Nb as a function of solid fraction predicted by three different methods.

(iv) Influence of different thermodynamic database on the predicted properties

The available commercial Ni-database and Du et al's database [1] are used to probe the influences of different databases on the predicted properties including the Gibbs energies of

solid and liquid phases, the solid/liquid (S/L) phase boundaries, and the partition coefficients of Cr and Nb, where a Ni-15Cr-4.5Nb (wt.%) alloy is selected as the model alloy.

Fig. 7 shows the calculated Gibbs energies of solid and liquid phases of Ni-15Cr-4.5Nb by using the Ni-database and Du et al's database [1]. For both solid and liquid phases, the calculated Gibbs energies by Du et al's database shift to the lower positions with respect to those obtained from Ni-database, indicating that the solid phase predicted by Du et al's database should be more stable than that predicted by Ni-database. As a consequence, the S/(S+L) and (S+L)/L phase boundaries calculated by Du et al's database should occur at higher temperatures.

Fig. 8 illustrates the calculated S/(S+L) and (S+L)/L phase boundaries of Ni-15Cr-xNb and Ni-20Cr-xNb (wt.%) alloys by Ni-database and Du et al's database [1]. The differences of phase boundaries are clearly shown in Fig. 8.

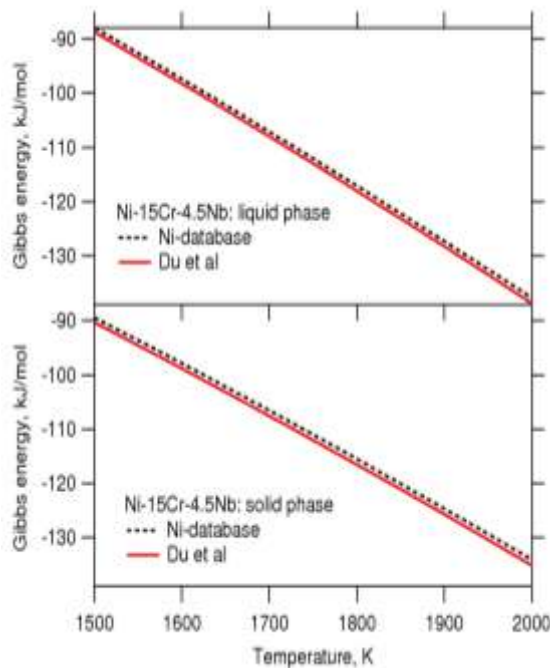


Fig. 7. Calculated Gibbs energies of solid and liquid phases of Ni-15Cr-4.5Nb (wt.%) by Ni-database and Du et al's database [1].

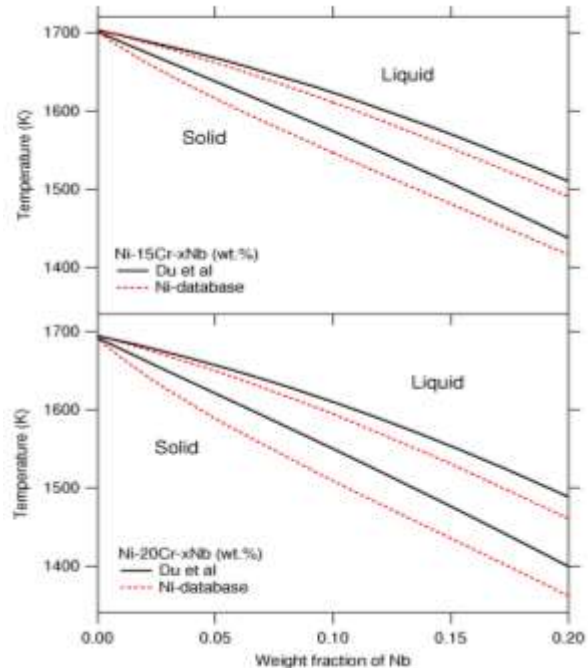


Fig. 8. Calculated solid/liquid phase boundaries of Ni-15Cr-xNb and Ni-20Cr-xNb (wt.%) by Ni-database and Du et al's database [1].

Fig. 9 gives the calculated phase transition temperatures and the partition coefficients of Cr and Nb as function of solid fraction for Ni-15Cr-4.5Nb (wt.%) alloy, wherein both the Ni-database and Du et al's database [1] are used, and three kinds of solidification models are employed as follows: 1) the equilibrium solidification via lever rule, 2) Scheil model, and 3) back diffusion model by DICTRA software, where the cooling rate 10K/min is employed.

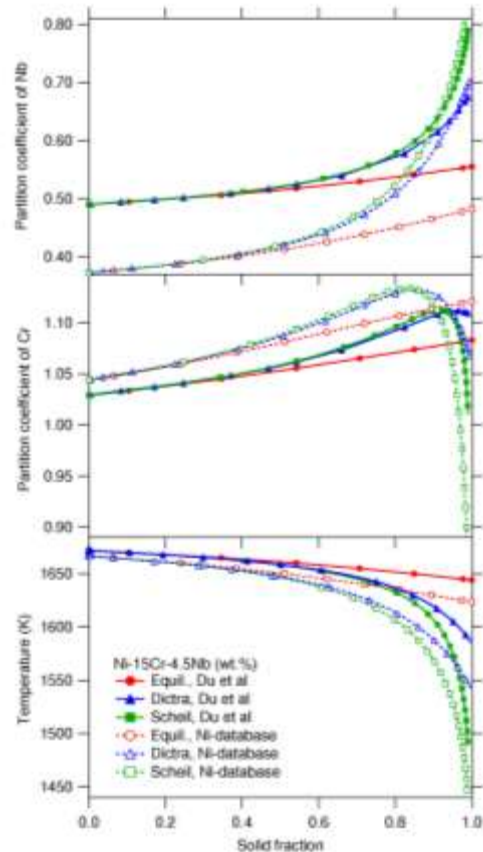


Fig. 9. Calculated phase transition temperatures and partition coefficients of Cr and Nb as function of solid fraction in Ni-15Cr-4.5Nb (wt.%).

Fig. 9 shows that the different databases (thermodynamic data) have large influences on the predicted phase transition temperatures and partition coefficients. Just as the phase boundaries shown in Fig. 8, the Ni-database predicts a lower phase transition temperatures with respect to those obtained by Du et al's database for all the three cases: equilibrium, Scheil and Dictra calculations. Regarding the predicted partition coefficients, the large differences present for the element Nb. The calculated partition coefficients of Nb by the Ni-database are lower than those obtained by Du et al's database (the difference is even larger than 0.1 at low solid fractions). Contrarily the predicted partition coefficients of Cr by Ni-database are higher than those obtained from Du et al's database.

(v) Partition coefficients of Cr and Nb in the Ni-Cr-Nb alloys

Predictions by Dictra simulations

Fig. 10 illustrates the calculated phase transition temperatures and the partition coefficients of Cr and Nb as a function of solid fraction in the Ni-15Cr-xNb and Ni-20Cr-xNb (wt.%) alloys by Dictra simulation (the back diffusion model). The thermodynamic data are taken from Du et al [1], the cooling rate are set as 10 K/min. With increasing Nb and/or Cr content, Fig. 10 indicates that the phase transition temperatures decrease. The contents of elements Nb and Cr have opposite influence on the calculated partition coefficients of Cr and Nb. With increasing Nb content, the partition coefficients of both Cr and Nb increase for each fixed solid fraction, while

with increasing Cr content the partition coefficients of Cr and Nb decrease. It should be remarked that the equilibrium calculation and the Scheil model will give the same trends as those obtained by Dictra calculation. The same trends still hold by using the Ni-database.

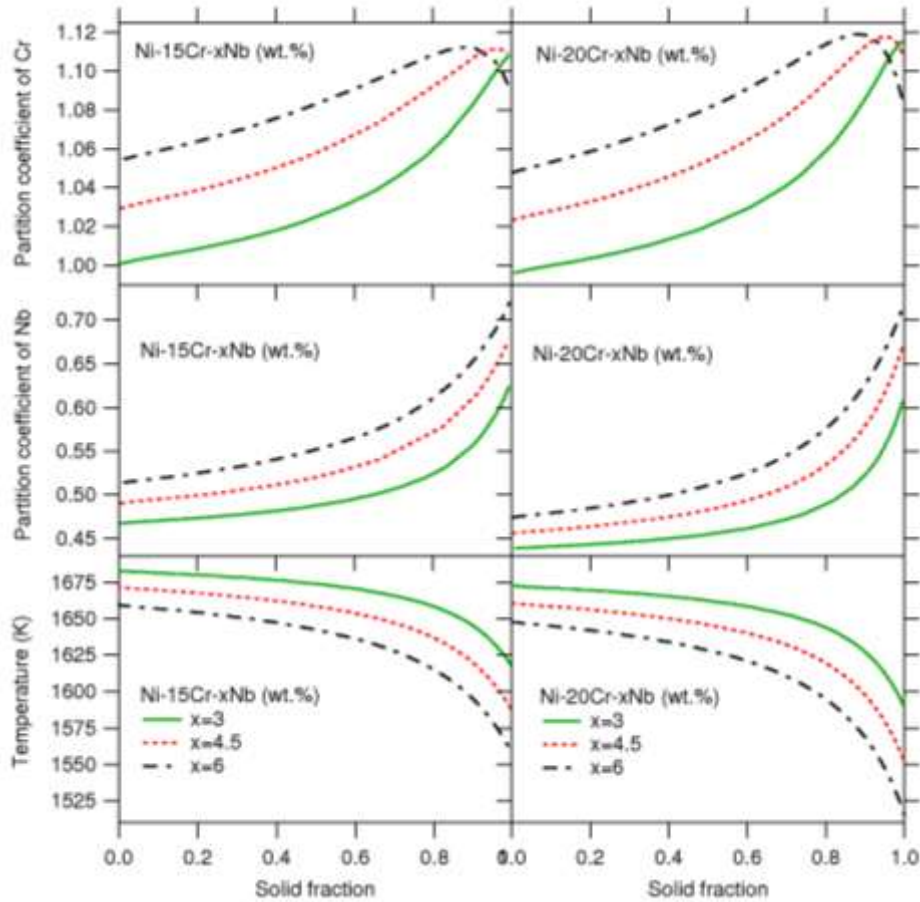


Fig. 10. Calculated phase transition temperatures and partition coefficients of Cr and Nb as function of solid fraction in Ni-15Cr-xNb and Ni-20Cr-xNb (wt.%) by Dictra simulation.

(vi) Partition coefficients of Fe and Nb in the Ni-Fe-Nb alloys

Predictions by equilibrium calculations

Fig. 11 illustrates the calculated phase transition temperatures and the partition coefficients of Fe and Nb as function of solid fraction in the Ni-18Fe-3Nb (wt.%) alloy by equilibrium calculations. The thermodynamic data are taken from this work and the commercial database [15], respectively. The present partition coefficient of Nb and phase transition temperatures are lower than for the commercial database while the partition coefficient of Fe is higher. It shows the opposite trend to the result in the Ni-15Cr-4.5Nb alloy by equilibrium calculation (see Figs. 5, 6, 10). It indicates that the contributions of Fe and Cr elements to the whole system have large differences. It should be mentioned again that the diffusions of alloying elements in the liquid and solid phases are assumed to be infinitely fast in the equilibrium solidification.

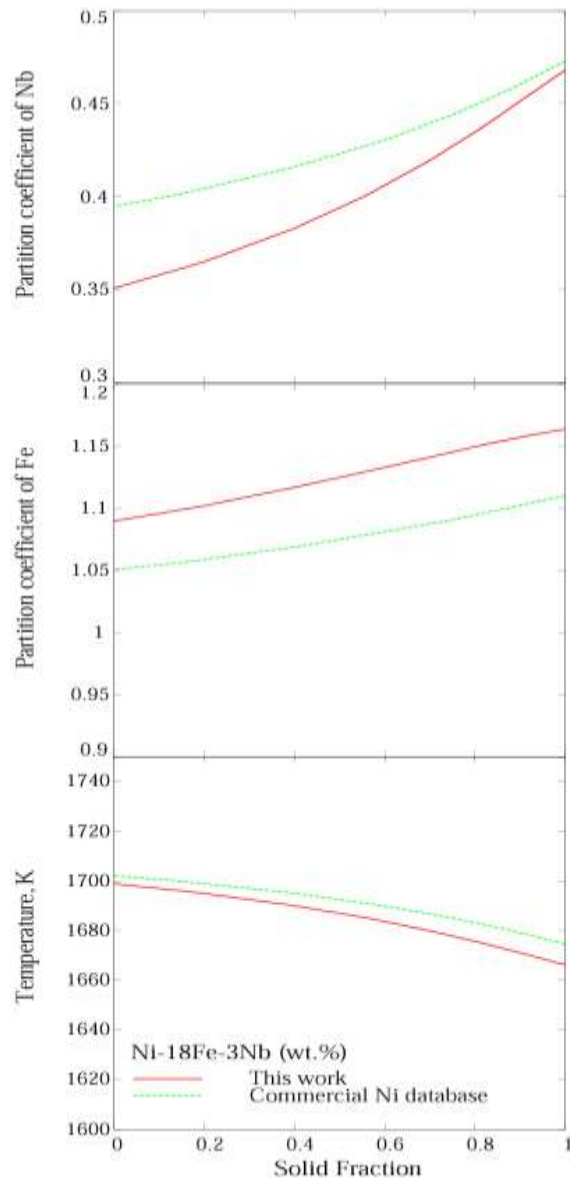


Fig. 11. Calculated phase transition temperatures and partition coefficients of Fe and Nb as function of solid fraction in Ni-18Fe-3Nb (wt.%)

Fig. 12 shows the effects of Fe and Nb content in the Ni-Fe-Nb system on the partition coefficients and the phase transition temperatures. With increasing of Nb, both partition coefficients of Fe and Nb increase and the phase transition temperature decreases. When the content of Fe increase the partition coefficient of Fe increase only while the partition coefficient of Nb and the phase transition temperature decrease.

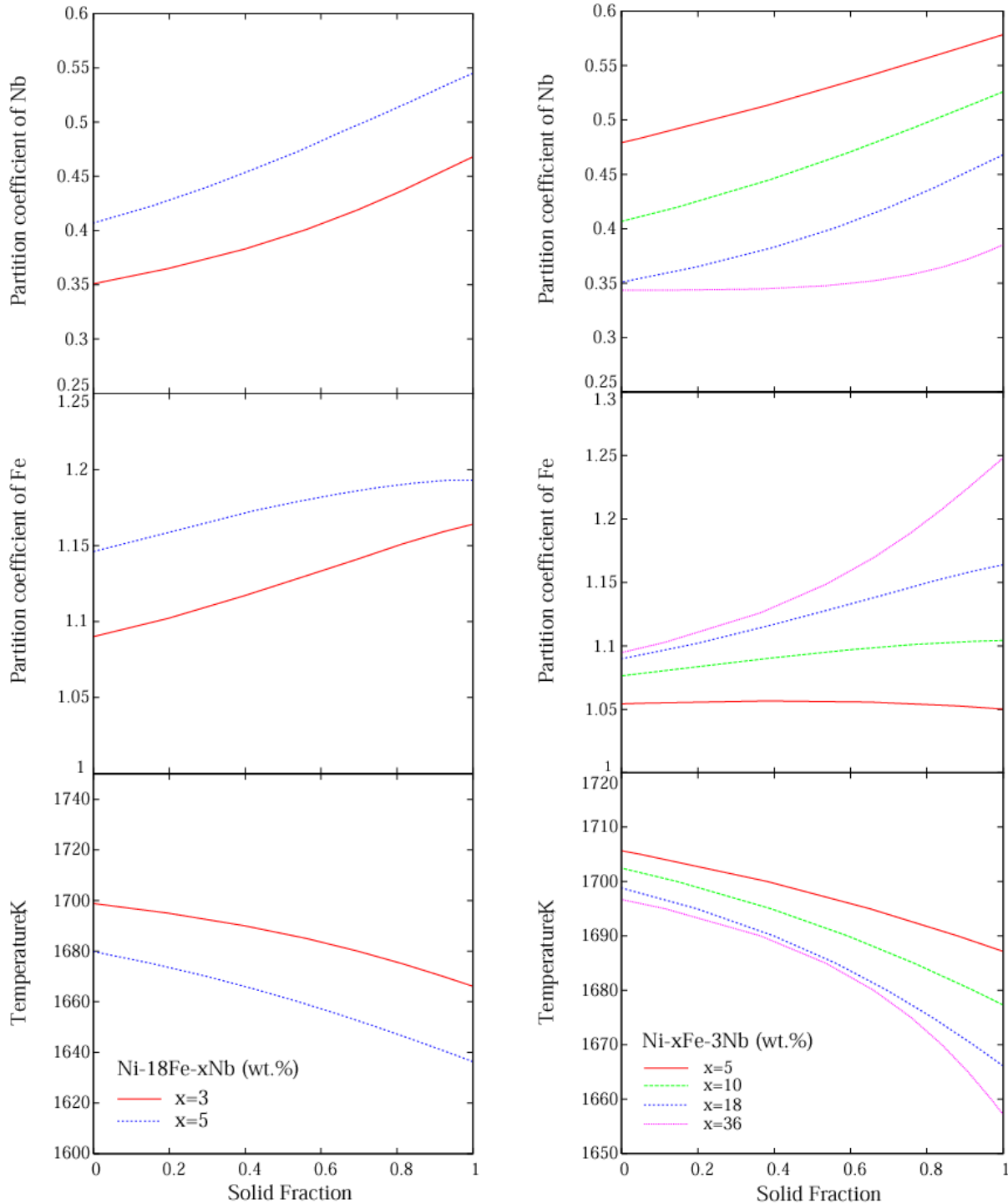


Fig. 12. Calculated phase transition temperatures and partition coefficients of Fe and Nb as a function of solid fraction in the Ni-18Fe-xNb (left) and Ni-xFe-3Nb (right) (wt.) by equilibrium calculations.

(vii) Partition coefficients of interstitial element C in the Ni-C-Cr-Nb alloys

The influences of C content on the transition temperature and the partition coefficients of Cr and Nb in Ni-15Cr-4.5Nb-xC and Ni-20Cr-4.5Nb-xC as a function of solid fraction by equilibrium

calculations are shown in Fig. 13. The thermodynamic data are obtained from the result of Du et al[1] and three binary systems including carbon, which are the Ni-C and Nb-C system by Lee[16] and the Cr-C system by Lee[16] and Bratberg[17]. Fig. 13 shows that, as increasing C content, the phase transition temperatures decreases and the partition coefficient of Cr also decreases, but the partition coefficient of Nb increases. It should be mentioned that the ternary interactions of the Ni-Cr-C, Ni-Nb-C or Cr-Nb-C system can not be considered because there is no information about those systems. However, the influence of C content on the Ni-Cr-Nb alloys still can be predicted using the database obtained.

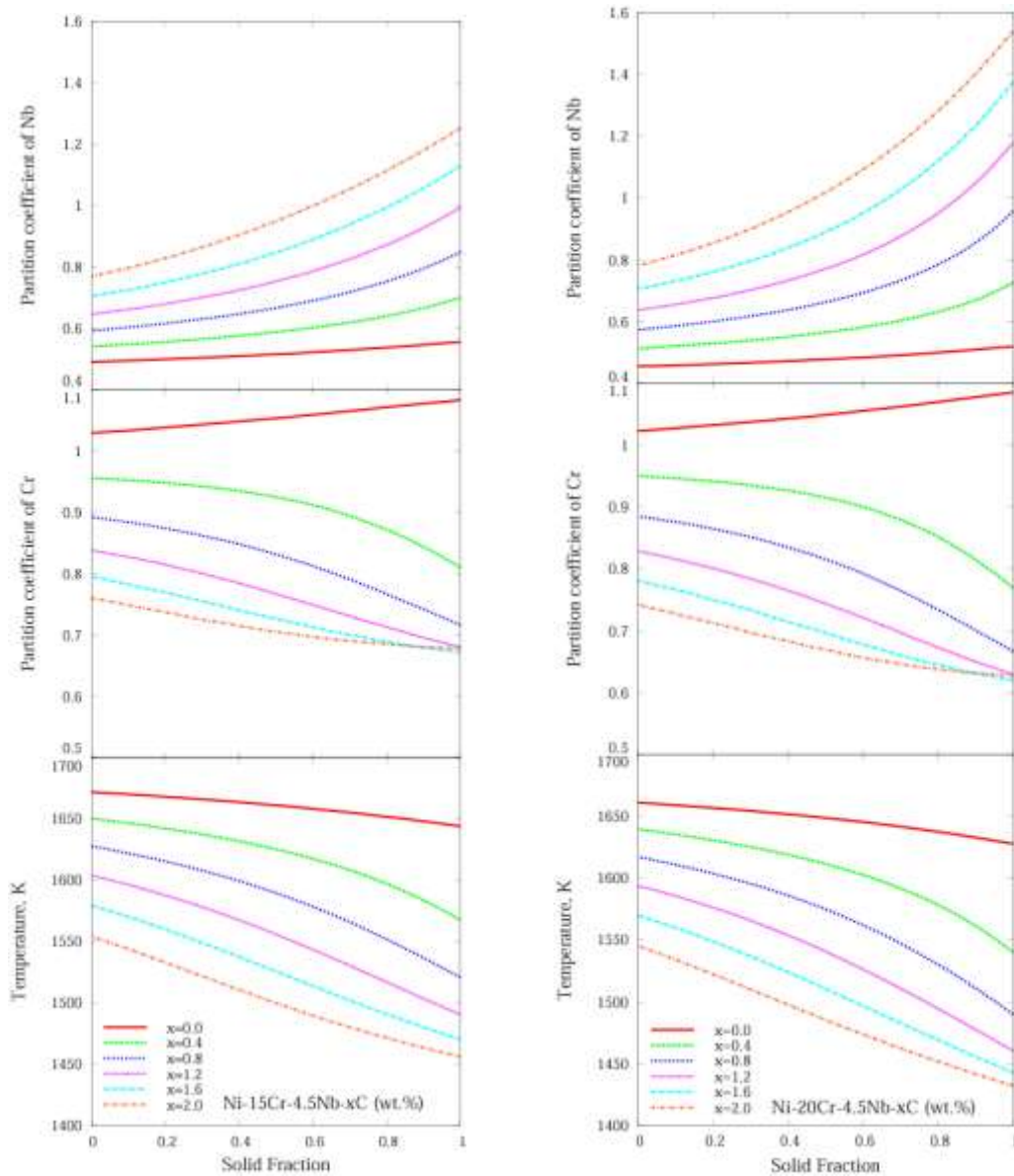


Fig.13. Calculated phase transition temperatures and partition coefficients of Cr and Nb as function of solid fraction in Ni-15Cr-4.5Nb-xC and Ni-20Cr-4.5Nb-xC (wt.%) by equilibrium calculations.

(viii) Build of ternary special quasirandom structures (SQSs) to be used in the first-principles calculations for disordered alloys.

The estimation of ternary interactions (such as in the Ni-Fe-Nb system) is crucial, especially for the FCC based γ phase with random mixing of elements such as Fe, Ni, and Nb. Due to the lack of experimental data in ternary Ni-Fe-Nb system, the first-principles calculations will be adopted to obtain the mixing of enthalpy for the random solution phase γ on the basis of the SQS's (special quasirandom structures). Note that, the ternary interactions used to calculate the Ni-Fe-Nb phase diagram (see Figs. 3 and 4) are arbitrary values.

SQS's are specially designed small unit-cell ordered structures with only a few (2–32) atoms per unit cell, which mimic the most relevant, near-neighbor pair and multisite correlation functions of random substitutional alloys. The essence of SQS is to find an **ordered** compound in order to mimic the properties of the corresponding **disordered** structure [18, 19]. Since a set of correlation functions (CFs) can be used to designate a structure [3, 4], the first step of SQS calculation is therefore to construct an ordered compound (the so called SQS) whose CFs are equal to (or close to) the corresponding CFs of the disordered structure. The second step is to perform the first principles calculation based on the constructed ordered compound, and then to investigate the properties of the corresponding disordered structure.

In the literature the available SQS's exist for binary FCC [18, 19], BCC [20] as well as HCP [21] structures. However, there are no available SQS's for ternary systems. We thus generated the SQS's for FCC based ABC alloy with 24 atoms per unit cell and A_2BC alloy with 32 atoms per unit cell. Fig. 14 illustrates both the SQS's for ABC and A_2BC .

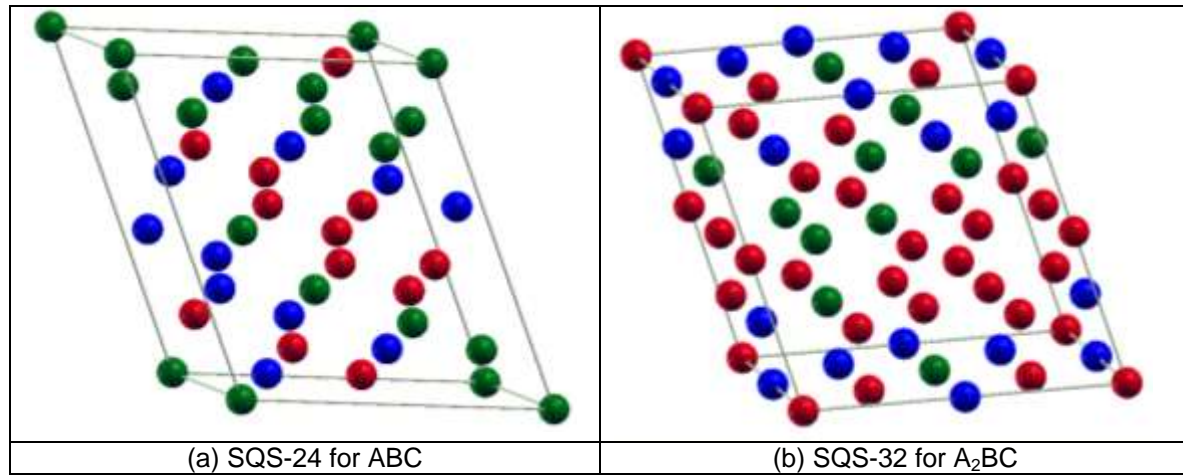


Fig. 14. FCC based SQS's for ternary compounds ABC with 24 atoms per unit cell (a), and A_2BC with 32 atoms per unit cell (b). The red balls represent the A atoms, blue the B atoms, and green the C atoms.

The details of the lattice vectors and the atomic positions for SQS-24 (ABC) and SQS-32 (A_2BC) are given in Table 2. The analysis of their correlation functions with respect to the real random alloys is given in [22].

Table 2. Lattice vectors and atomic positions for FCC based SQS-24 (ABC) and SQS-32 (A_2BC) in the Cartesian coordinates, there the lattice parameter equals to 4 is assumed for the original FCC structure.

SQS-24 (ABC)				SQS-32 (A_2BC)			
Lattice vectors				Lattice vectors			
X	12	4	-4	X	12	4	-4
Y	-12	4	-4	Y	-12	4	-4

Z	0	2	2	Z	0	2	2
Atoms	Atomic positions			Atoms	Atomic positions		
A	0	6	-2	A	0	6	-2
A	2	2	0	A	2	2	0
A	-2	4	-2	A	-2	4	-2
A	2	8	-6	A	2	8	-6
A	-4	6	-2	A	-4	6	-2
A	4	6	-2	A	4	6	-2
A	-4	8	-4	A	-4	8	-4
A	-6	4	-2	A	-6	4	-2
B	0	8	-4	A	0	8	-4
B	2	4	-2	A	2	4	-2
B	-2	8	-6	A	-2	8	-6
B	-4	4	0	A	-4	4	0
B	4	8	-4	A	4	8	-4
B	6	4	-2	A	6	4	-2
B	-6	6	-4	A	-6	6	-4
B	6	6	-4	A	6	6	-4
C	0	10	-6	B	0	10	-6
C	0	4	0	B	0	4	0
C	-2	2	0	B	-2	2	0
C	-2	6	-4	B	-2	6	-4
C	2	6	-4	B	2	6	-4
C	4	4	0	B	4	4	0
C	-8	6	-2	B	-8	6	-2
C	8	6	-2	B	8	6	-2
				C	0	10	-6
				C	0	4	0
				C	-2	2	0
				C	-2	6	-4
				C	2	6	-4
				C	4	4	0
				C	-8	6	-2
				C	8	6	-2

Sub-task 1.1.2 Experimental Investigation on Partition Coefficients (Liu/WVU)

The solute elements included in the experimental investigation of the partition coefficients included major elements like Chromium and Iron, which form solid solution in the gamma phase, and minor elements that provide precipitation strengthening at high temperatures, specifically Nb (γ'' : Ni₃(Nb, Al, Ti)), Al and Ti (γ' : Ni₃(Al, Ti)). The compositions were created to evaluate the compositional effects over the solidification reaction.

The set of model alloy samples was produced using the available arc bottom furnace as described in the quarterly reports submitted in the year 2006. Although the procedure included multiple steps of re-melting and two repetitions per alloy to ensure homogeneous samples in terms of chemical composition, naturally, variability was found.

CALPHAD theoretical simulations were performed using the equilibrium method and the Ni commercial database for all the model alloys prepared. Combinations of the minimum, maximum and average weigh percent of the alloying elements were simulated and the results

showed that the solidification curves always were confined by the ones corresponding to the alloys with the minimum and maximum solute elements content. (All levels of alloying elements at low or high values). Fig. 15 shows the limiting curves for alloys 3 and 6. The offset data for experimental solidus and liquidus temperatures are included. The measurements were found practically within the composition variability band of the respective alloy.

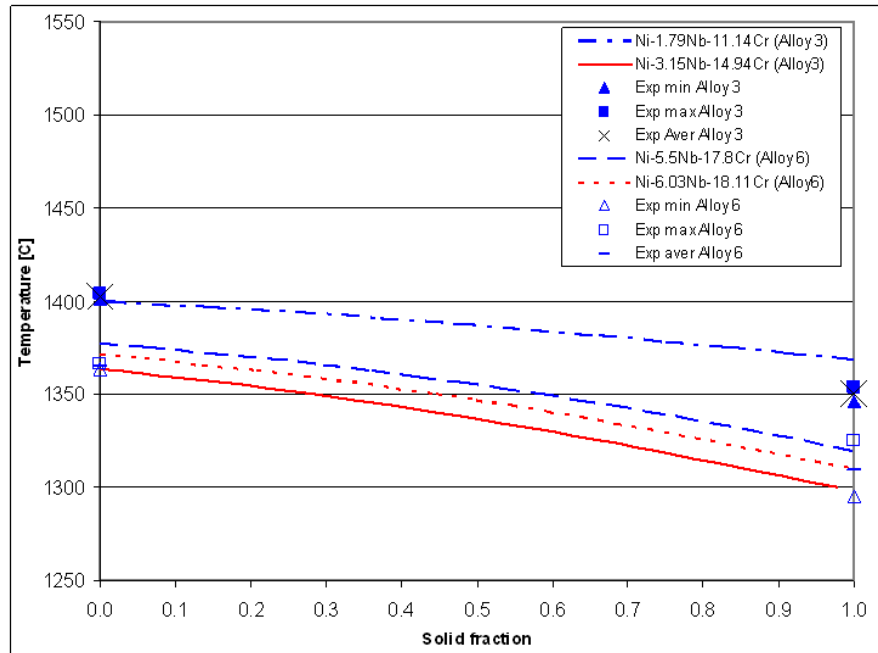


Fig.15. Comparison between Alloy 3 and Alloy 6.

Greater composition variability was observed for alloy 3, while its corresponding DTA measurements were found to be very consistent. This is particularly important because if the variability of the chemical composition in this case didn't increased the DTA data range could mean that the lack of homogeneity being observed from the large samples analyzed by SEM/EDX (~1 g) resembles a characteristic that extends to a scale larger than the average DTA sample size (150 mg).

The measured transition temperatures decreased from alloy 3 to alloy 6 showing the tendency of increasing amount of Chromium observed on the simulations (Fig. 10)

The area of the band formed between the solidification curves of the limiting alloys was used as a quantitative description of the variability of the chemical composition obtained for a particular model alloy. This area was defined as the composition variation index (CVI). The CVI was calculated for all the model alloys and the results are presented in the table 4.

Table 3. Composition Variation Index (CVI) for all model alloys included in the DTA experiments

Model alloy	Variation index	Subsystem
Alloy 13	59.6729833	Ni-Fe-Nb
Alloy 11	59.14455	Ni-Fe-Nb
Alloy 3	51.3136333	Ni-Cr-Nb
Alloy 2	47.0911667	Ni-Cr-Nb
Alloy 15	43.37935	Ni-Cr-Fe-Nb
Alloy 5	26.1025	Ni-Cr-Nb

Alloy 1	25.176166	Ni-Cr-Nb
Alloy 16	17.1515	Ni-Cr-Fe-Nb
Alloy 4	15.9701	Ni-Cr-Nb
Alloy 17	11.8433333	Ni-Cr-Fe-Nb
Alloy 8	11.5844667	Ni-Fe-Nb
Alloy 10	10.1655333	Ni-Fe-Nb
Alloy 6	8.22266667	Ni-Cr-Nb
Alloy 18	7.555	Ni-Cr-Fe-Nb
Alloy 9	5.0035	Ni-Fe-Nb
Alloy 20	4.5724	Ni-Cr-Al
Alloy 12	4.07383333	Ni-Fe-Nb
Alloy 28	4.00445	Ni-Cr-Ti
Alloy 27	3.91481667	Ni-Cr-Ti
Alloy 21	3.56265	Ni-Cr-Al
Alloy 29	2.64853333	Ni-Cr-Ti
Alloy 7	2.43953333	Ni-Fe-Nb
Alloy 19	1.548	Ni-Cr-Al
Alloy 14	~0	Ni-Fe-Nb
Alloy 22	~0	Ni-Cr-Al
AVERAGE	19.154	
STDDEV	19.55	

DTA experiments included cooling rates of 3, 5, 10 and 25 °C/ min depending on the characteristics of the curves in regards to the shape of the transition peaks and amount of shifting due to superheating or undercooling effects. All of the DTA experiments were performed using ultra high purity Argon as protective atmosphere.

Considering that the simulations using CALPHAD methodology show that the influence of the interactions between elements above the ternary subsystems do not affect considerably the free energy [23], [24], and hence the thermal properties like the solidus and liquidus temperatures, the DTA experiments for the quaternary subsystems were temporally excluded and emphasis was given to the model alloys of the ternary subsystems.

Only the Ni-Cr-Fe-Nb quaternary subsystem was currently included. The optimized use of the DTA instrument permitted designing an experimental plan including quenching DTA experiments for all ternary subsystems form the total set of model alloys proposed.

The set of experimental DTA data showed variability that could be decomposed in different contributions. First, a contribution could be associated with human, instruments and methodology induced errors, which can be regarded as represented by a random variable. Also, a variation in the collected data is related to the changes in the nature of the samples, which mainly correspond to the changes in the chemical compositions.

In most of the cases the measured solidus and liquidus temperatures revealed these two variations when evaluating between different model alloys.

Finally, a variation contribution was observed in some of the subsystems that was not related to the change in the nature of the alloys, or related to the experimental methodology. This variation was better described as a divergence from the theoretical expected values that resembled the typical behavior observed when instruments are not correctly calibrated. Because the calibration step was always performed to accuracy within 2 °C (High purity Nickel standards used, Tm:1455 °C), before evaluating each subsystem, the difference observed was regarded

as an offset and a physical meaning should be found. Nevertheless, It's important to point out that, when the data is filtered subtracting the offset (which always was positive), the experimental data follows the tendency of variation of the theoretical predictions associated to the nature of the alloys, in other words, associated to the chemical composition changes. For this document, experimental data refers to raw measured values, unless "offset data" is specified and subtraction of the offset value is assumed.

A) Effect of the alloying elements on the transformation temperatures

The variations of the major solute elements not only affected the transformation temperatures but also had incidence on the composition variability Index (CVI) of the samples. The following discussion presents the observations that supported the experimental description of the partition coefficients, which are outmost importance in understanding/preventing macro segregation defects.

(i) Subsystem Cr-Ni-Nb

When comparing the alloy 1 with alloy 4, the major change in the chemical composition was the increase in the amount of Chromium since the Niobium change was noticeably smaller, as can be observed in the fig. 16. Ni ranges overlap by 0.68 Wt%, while Cr ranges differ for at least 1.56 Wt%

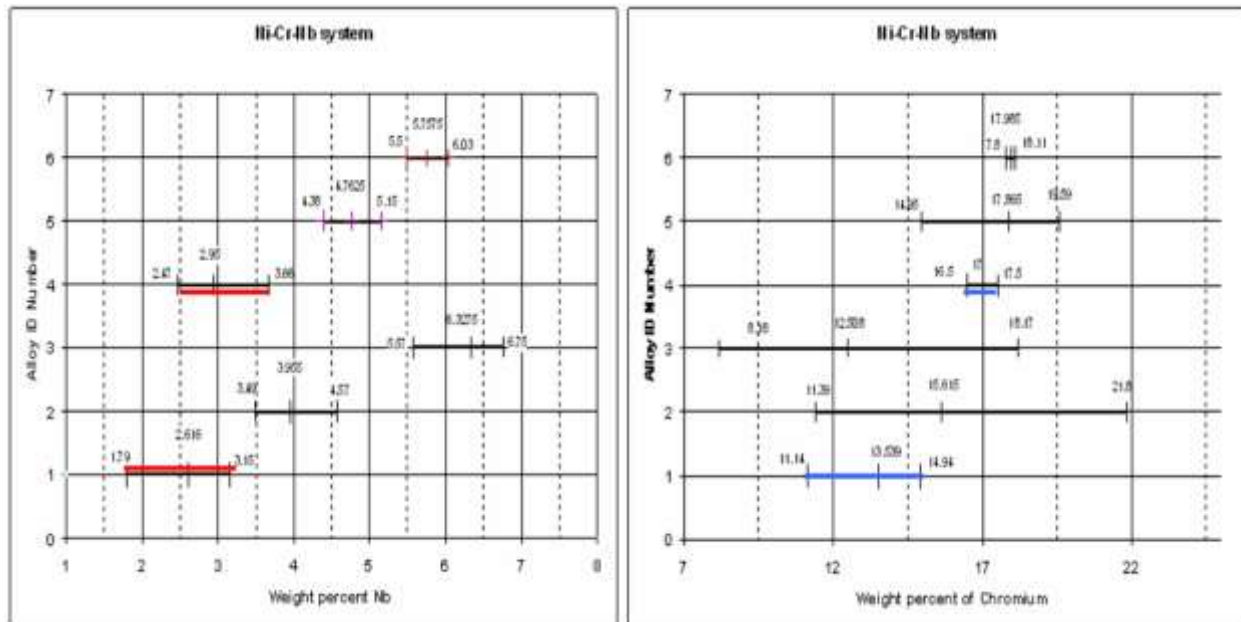


Fig.16. Relations between the chemical compositions for the model alloys obtained in the subsystem Cr-Ni-Nb

When increasing the amount of Cr from alloy 1 to alloy 4, the effect on solidification characteristics manifested as a slight decrease in the offset experimental solidus and liquidus temperatures (averages ΔT_{liq} : - 6 °C, ΔT_{Sol} : -9 °C), in agreement to the tendency predicted by the equilibrium method simulation (ΔT_{liq} :-9.2 °C , ΔT_{Sol} :-17 °C). The experimental offset data suggest also that the samples, although extracted from different intended model alloys,

pertained to the region on which the two variability bands overlap as observed in fig.17, and the difference in Chromium might not be enough to show its effect on higher magnitude as when comparing between alloy 3 and alloy 6 (fig.18). Another useful comparison was performed between alloy 4 and alloy 6 given the fact that their Chromium content was similar and presented higher difference in the amount of Niobium (Wt% Cr of both alloys within a range of 1.61 Wt%; Δ Wt% Nb \geq 1.84 Wt %). The DTA experimental offset data was found to closely follow the tendency of the theoretical equilibrium simulations and the increase in Niobium decreased the measurements magnitudes accordingly. The composition variability indexes (CVI's) of the alloys 4 and 6 were of magnitudes differing by less than 5 units [wt%].

The change of composition between model alloy 11 to model alloy 13, was essentially an increase of the Iron content from around 18 to approximately 36 Wt.%, while the Nb content was kept almost constant (3.53 Wt% Nb overlap) . The effect of increasing the Fe content was increasing the transformation temperatures as observed in the DTA experiments, and this tendency was confirmed in the theoretical equilibrium calculation.

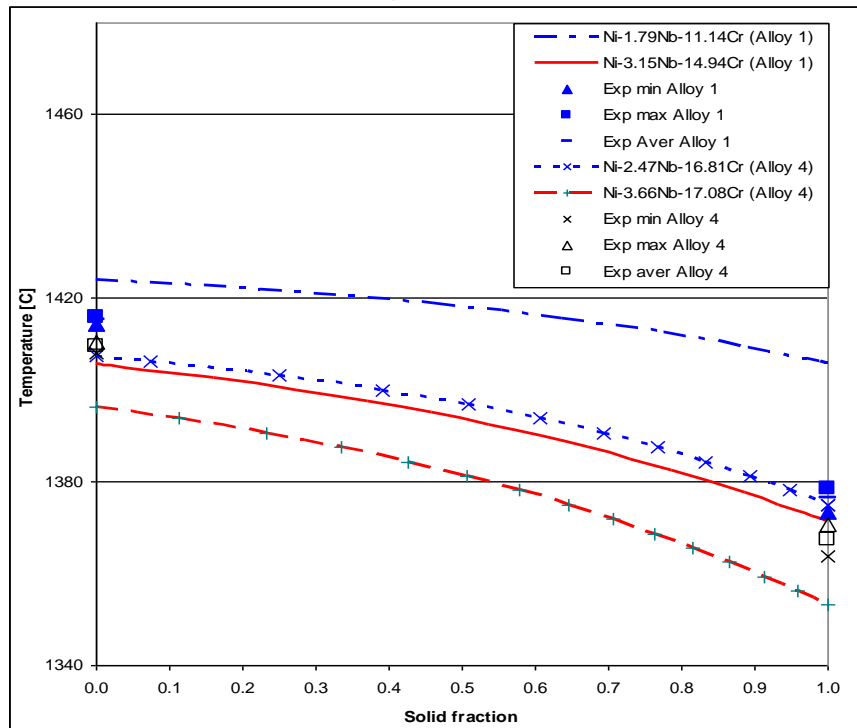


Fig.17. Comparison between Alloy 1 and Alloy 4 results

Based on the detailed experimental results for the Cr and Nb compositions in the Ni-Cr-Nb alloys, the temperatures of the solidus and liquidus for the “fcc + liquid” phase region have been predicted using the following three methods: (1) the equilibrium calculations via the lever rule; (2) the back diffusion model implemented in the Dictra software, the cooling rate is 10 K/min, and (3) the Scheil’s model.

For each Ni-Cr-Ni alloy, the measured minimum and maximum Cr and Nb compositions are used in the predictions. The thermodynamic/kinetic databases are Du’s and NISTmob, respectively. The calculated solidus and liquidus temperatures are given in Table 4. The comparisons between the raw measured (average) temperatures and the predicted minimum and maximum temperatures of solidus and liquidus are shown in Fig. 18.

Table 4. Measured and calculated solidus and liquidus temperatures of the Ni-Cr-Nb alloys.

		Nb (wt. %)	Cr (wt. %)	Solidus (K)	Liquidus (K)
Alloy-1	Measured (average)			1709.49	1725.80
	Lever Rule (EQ)	1.79	11.14	1686.86	1698.76
	Lever Rule (EQ)	3.15	14.94	1661.13	1682.19
	Dictra 1/6 K/sec	1.79	11.14	1656.64	1700.96
	Dictra 1/6 K/sec	3.15	14.94	1612.53	1683.46
	Scheil	1.79	11.14	1604.15	1698.76
	Scheil	3.15	14.94	1528.55	1682.19
Alloy-2	Measured (average)			1698.73	1721.68
	Lever Rule (EQ)	3.49	11.39	1666.41	1686.59
	Lever Rule (EQ)	4.57	21.8	1620.30	1656.20
	Dictra 1/6 K/sec	3.49	11.39	1622.68	1688.46
	Dictra 1/6 K/sec	4.57	21.8	1535.99	1658.46
	Scheil	3.49	11.39	1547.55	1686.59
	Scheil	4.57	21.8	1412.75	1656.20
Alloy-3	Measured (average)			1683.67	1713.10
	Lever Rule (EQ)	5.57	8.18	1651.88	1677.20
	Lever Rule (EQ)	6.75	18.17	1603.49	1645.94
	Dictra 1/6 K/sec	5.57	8.18	1604.51	1678.46
	Dictra 1/6 K/sec	6.75	18.17	1513.49	1645.96
	Scheil	5.57	8.18	1526.95	1677.20
	Scheil	6.75	18.17	1393.75	1645.94
Alloy-4	Measured (average)			1700.47	1720.12
	Lever Rule (EQ)	2.47	16.81	1664.90	1683.43
	Lever Rule (EQ)	3.66	17.08	1648.48	1674.01
	Dictra 1/6 K/sec	2.47	16.81	1618.78	1683.46
	Dictra 1/6 K/sec	3.66	17.08	1590.09	1675.96
	Scheil	2.47	16.81	1537.55	1683.43
	Scheil	3.66	17.08	1492.55	1674.01
Alloy-5	Measured (average)			1685.54	1713.89
	Lever Rule (EQ)	4.38	14.95	1645.67	1672.89
	Lever Rule (EQ)	5.15	19.59	1620.04	1656.48
	Dictra 1/6 K/sec	4.38	14.95	1587.44	1673.46
	Dictra 1/6 K/sec	5.15	19.59	1539.08	1658.46
	Scheil	4.38	14.95	1491.75	1672.89
	Scheil	5.15	19.59	1420.35	1656.48
Alloy-6	Measured (average)			1642.61	1675.26
	Lever Rule (EQ)	5.5	17.8	1621.72	1657.64
	Lever Rule (EQ)	6.03	18.11	1613.46	1652.40
	Dictra 1/6 K/sec	5.5	17.8	1544.89	1658.46
	Dictra 1/6 K/sec	6.03	18.11	1530.44	1653.46
	Scheil	5.5	17.8	1431.15	1657.64
	Scheil	6.03	18.11	1413.35	1652.40
Alloy-1 (first from the first batch, Ignoring C content)	Measured (average)			1669.23	1714.31
	Lever Rule (EQ)	1.83	8.88	1691.19	1702.49
	Lever Rule (EQ)	2.97	9.54	1676.92	1693.69
	Dictra 1/6 K/sec	1.83	8.88	1655.32	1703.46
	Dictra 1/6 K/sec	2.97	9.54	1640.18	1695.96
	Scheil	1.83	8.88	1615.35	1702.49
	Scheil	2.97	9.54	1575.55	1693.69

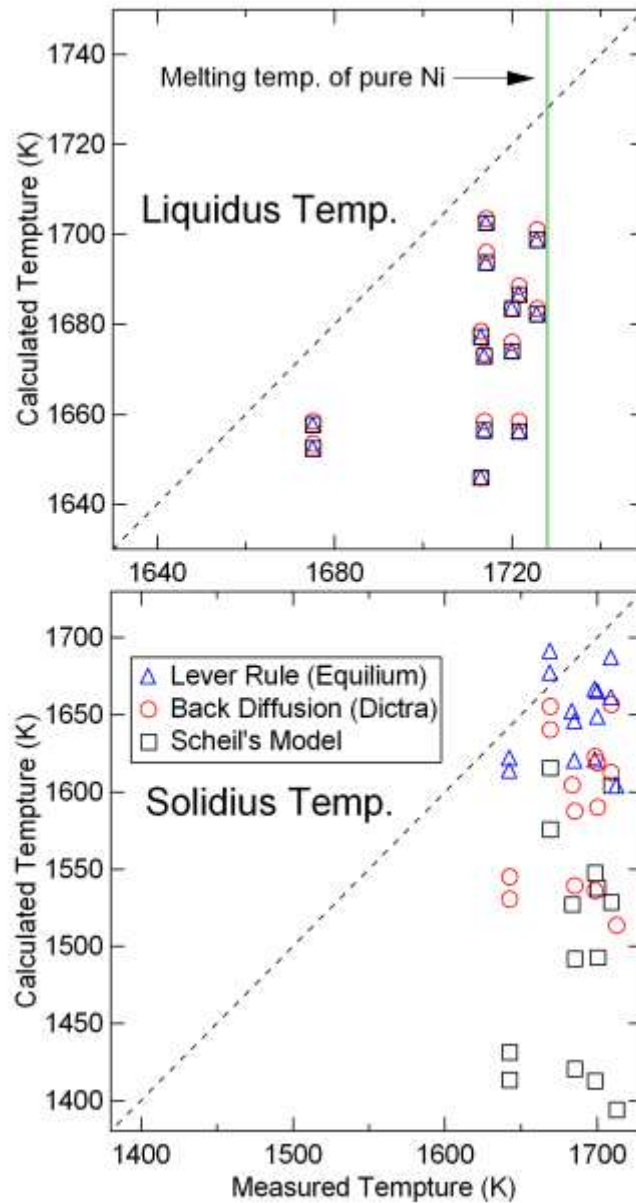


Fig. 18. Measured (average values) and calculated liquidus (up panel) and solidus (down panel) temperatures of the Ni-Cr-Nb alloys.

Table 4 and Fig. 18 show that the measured liquidus and solidus of the Ni-Cr-Nb alloys are in general agreement with the predictions. Regarding the liquidus, the different methods (lever rule, back diffusion, and Scheil model) predict almost the same temperature at each fixed composition, and the measured temperatures of liquidus are 10~40 K higher than those by calculations. These differences (10~40 K) are usually acceptable by considering the errors from the equipments and samples, and also the difficult of measurement for liquidus. It also should be mentioned that the presently predicted temperatures of liquidus are different to measurements due to the facts of (1) the melting point for pure Ni is 1728 K (see Fig. 18), and (2) the addition of Cr and/or Nb in Ni-alloy decreases the melting temperature of pure Ni as

shown in Fig. 19: the calculated phase diagrams of Ni-Cr and Ni-Nb systems. It is shown that the adding of Nb decreases quickly the solidus and liquidus than that of Cr. As a rough estimation, the temperatures of solidus and liquidus decrease ~ 1 K by adding of 1 wt.% Cr, and ~ 3 K by adding of 1 wt.% Nb.

Regarding the solidus, the predictions as shown in Fig.1 and Table 1 are in good agreement with the measurements, in particular the calculations by lever Rule and the back diffusion model with cooling rate of 10 K/min.

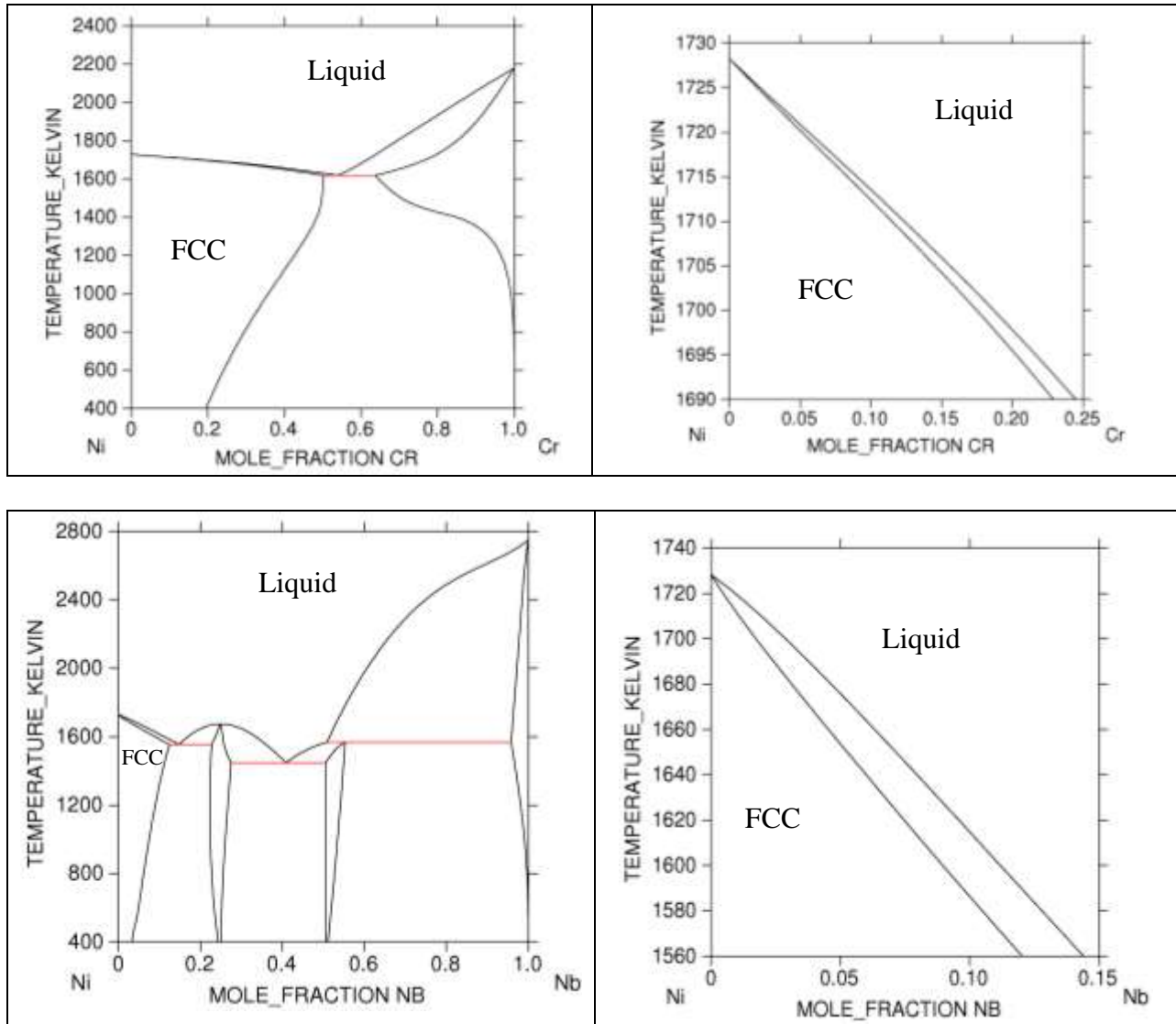


Fig. 19. Calculated phase diagrams of the Ni-Cr (up panels) and Ni-Nb systems together with the enlarged FCC+Liquid phase regions

(ii) Subsystem Fe-Ni-Nb

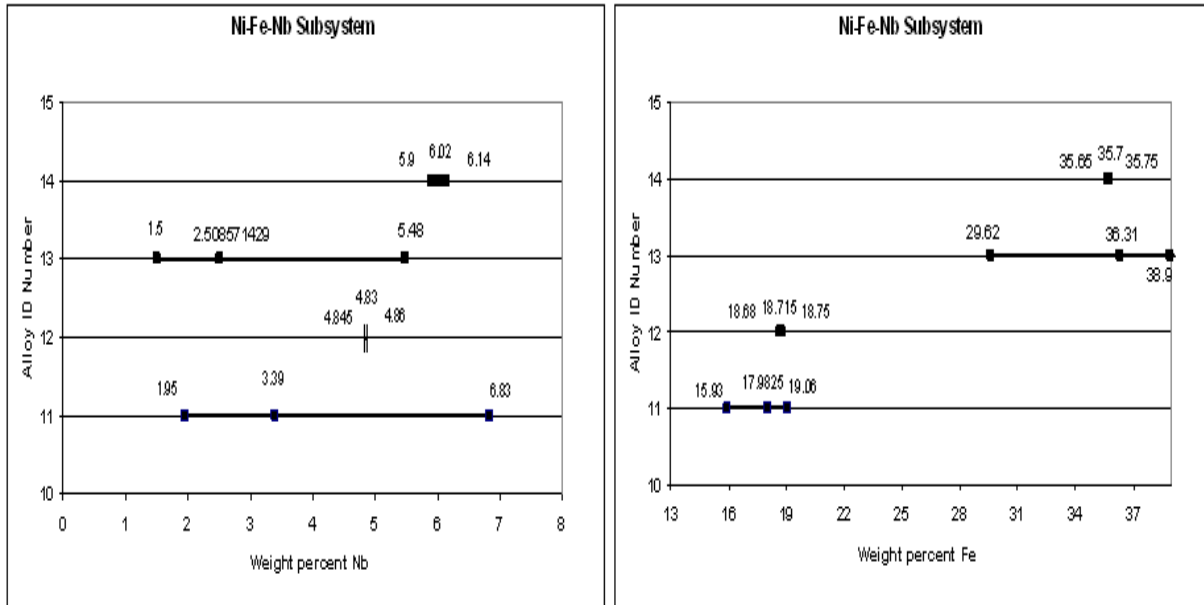


Fig.20 Relations between the chemical compositions for the model alloys obtained in the subsystem Fe-Ni-Nb

Using the data collected for Fe and Nb contents in the Ni-Fe-Nb alloys presented in Fig.21, the temperatures of the solidus and liquidus for the “fcc + liquid” phase region have been predicted using the equilibrium calculation via the lever rule.

For each Ni-Fe-Nb alloy, the measured minimum and maximum values of the Fe and Nb compositions were used in the predictions. The thermodynamic database is from this work. The calculated solidus and liquidus temperatures are given in Table 3. The comparisons between the measured (average) temperatures and the predicted minimum and maximum temperatures of solidus and liquidus are shown in Fig. 21.

Table 5 and Fig. 21 show that the most of measured temperatures of liquidus are 10~50 K higher than those by calculations. These differences (10~50 K) are usually acceptable by considering the errors caused by the equipments and samples, and also the difficulty of measurement for liquidus. It also should be noticed that the predicted temperatures of liquidus are better than the experimental data because the temperatures of the most of measurements are over 1728K, which is the melting point of pure Ni. The melting temperatures of alloys with Fe and Nb in the pure Ni should be lower than that of the pure Ni. Regarding the solidus temperature, the predictions as shown in Fig. 5 and Table 3 are 1~100 K lower than the measurements.

Table 5. Measured and calculated solidus and liquidus temperatures of the Ni-Fe-Nb alloys.

		Nb (wt. %)	Fe (wt. %)	Solidus (K)	Liquidus (K)
Alloy-7	Measured (average)			1732.35	1752.73
	Lever Rule (EQ)	3.46	4.66	1682.77	1702.07
	Lever Rule (EQ)	4.67	5.58	1666.91	1690.69
Alloy-8	Measured (average)			1692.15	1730.77
	Lever Rule (EQ)	3.45	4.66	1682.88	1702.15

Alloy-9	Lever Rule (EQ)	4.67	5.36	1667.54	1690.94
	Measured (average)			1694.78	1732.37
Alloy-10	Lever Rule (EQ)	3.35	10.41	1671.91	1698.99
	Measured (average)			1713.02	1728.27
Alloy-11	Lever Rule (EQ)	6.01	9.96	1639.00	1673.44
	Lever Rule (EQ)	6.02	9.98	1638.83	1673.33
	Measured (average)			1731.99	1734.441
Alloy-12	Lever Rule (EQ)	1.95	15.93	1685.14	1708.98
	Lever Rule (EQ)	6.83	19.06	1608.58	1661.24
	Measured (average)			1729.5	1735.023
Alloy-13	Lever Rule (EQ)	4.83	18.68	1637.84	1681.34
	Lever Rule (EQ)	4.86	18.75	1637.31	1681.03
	Measured (average)			1687.42	1745.75
Alloy-14	Lever Rule (EQ)	1.5	29.62	1686.34	1707.68
	Lever Rule (EQ)	12.36	38.9	1487.94	1645.66
	Measured (average)			1709.37	1723.925
	Lever Rule (EQ)	5.9	35.65	1605.77	1677.58
	Lever Rule (EQ)	6.14	35.75	1601.62	1676.13

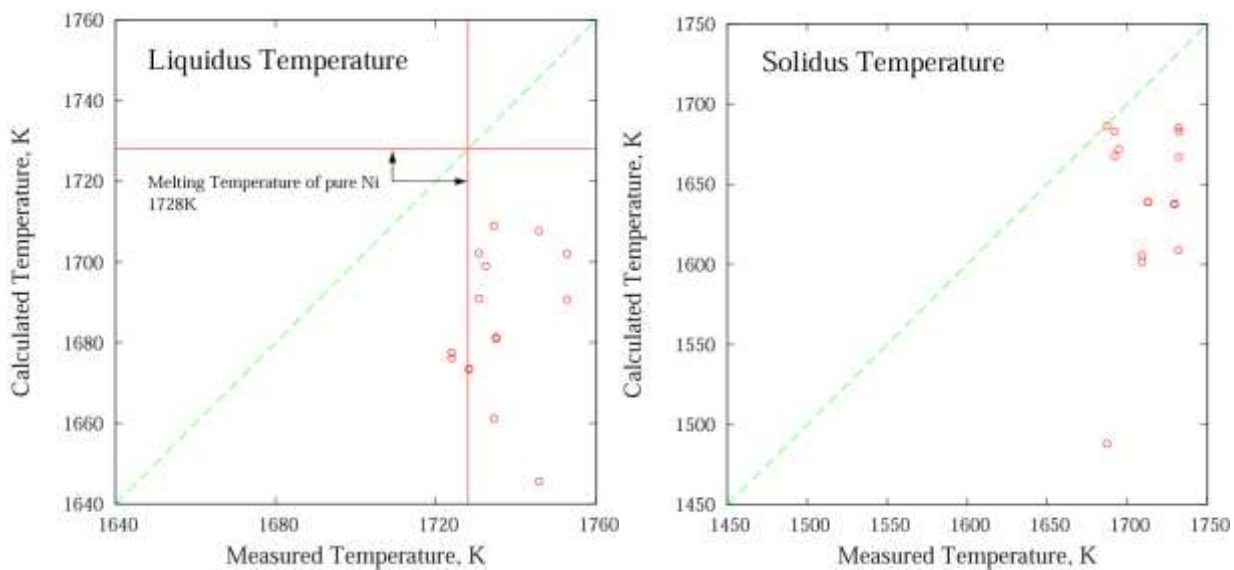


Fig. 21. Measured (average values) and calculated liquidus (left) and solidus (right) temperatures of the Ni-Fe-Nb alloys.

By making a dynamic comparison between the samples with the two lower levels of Fe, i.e. 5 and 10 Wt%, the variability of the DTA data showed the presence of the previously mentioned systematic variability considered as offset. When the data was corrected by $-47.9\text{ }^{\circ}\text{C}$ for Liquidus data and $-46.2\text{ }^{\circ}\text{C}$ for solidus, the experiments showed great agreement to the tendencies predicted by the equilibrium simulations as shown in fig. 22. It is important to reiterate that all experiments included at least one calibration, with pure nickel, per subsystem evaluated.

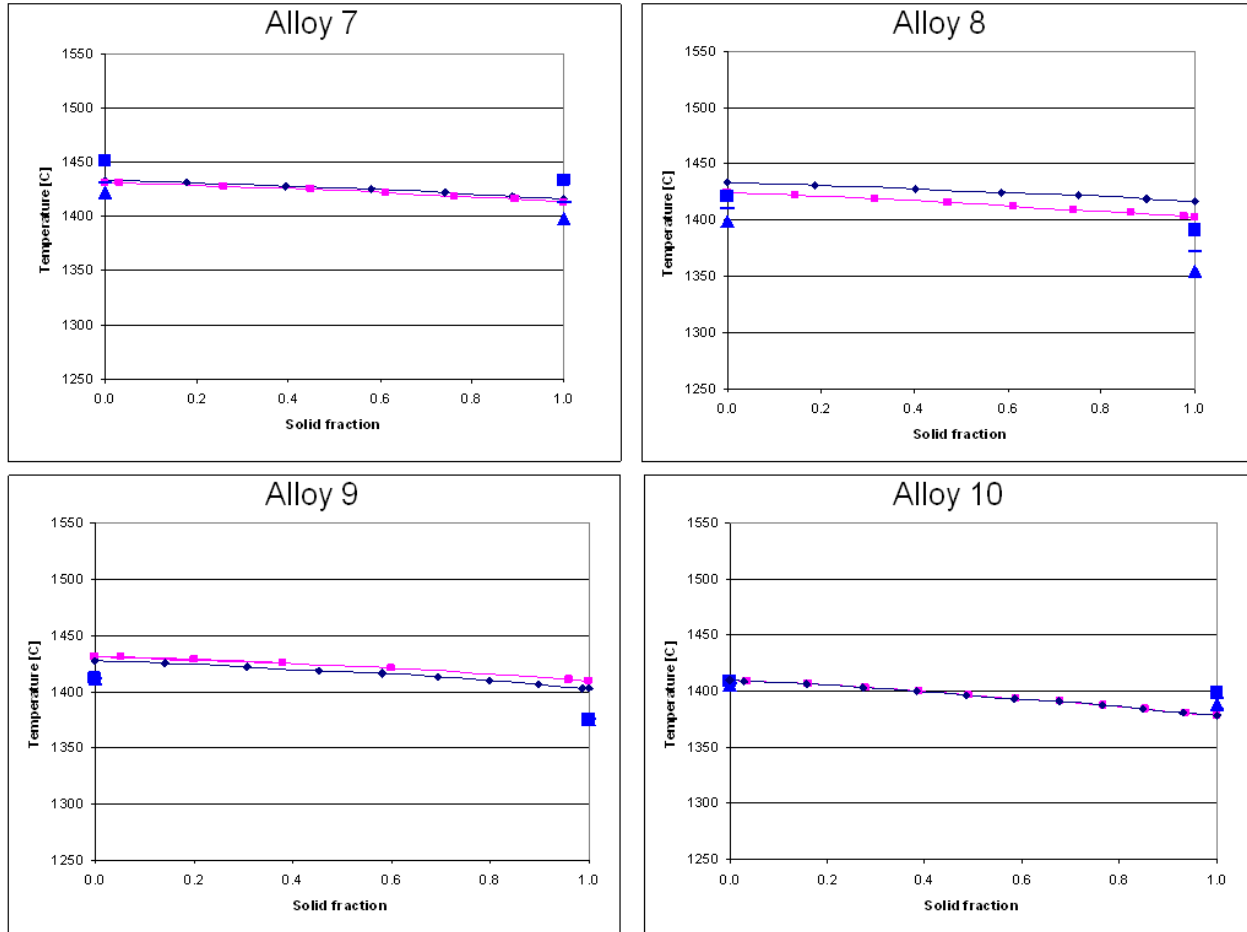


Fig. 22 Offset DTA data vs Equilibrium theoretical simulation for alloy subsystem Ni-Fe-Nb

(iii) Subsystem Cr-Ni-Al

Particularly, the DTA experimental results for the alloys of Ni-Cr-Al subsystem showed that the temperatures of solidus and liquidus were close in each case, showing narrow mushy zones similar to the one characteristic of the binary system Ni-Cr in fig. 24.

The effect of minor element Aluminum on the transformation of temperatures was not as evident as the observed for Nb.

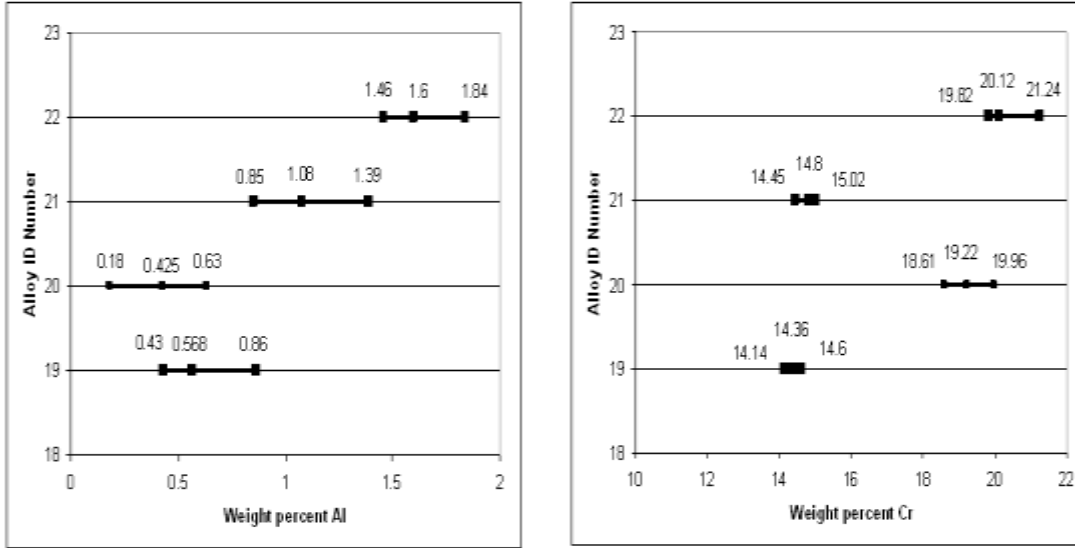


Fig. 23 Relations between the chemical compositions for the model alloys obtained in the subsystem Cr-Ni-Al

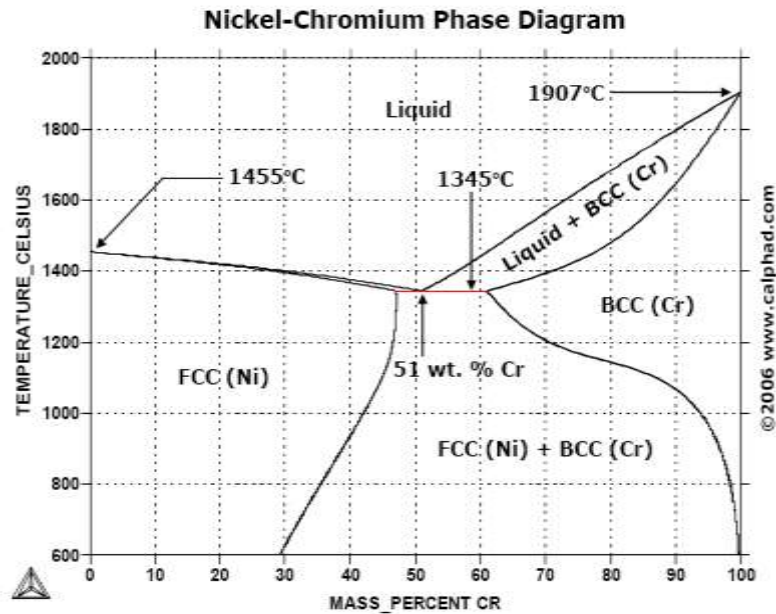


Fig.24 [25] Binary diagram Ni-Cr

(iv) Subsystem Cr-Ni-Ti

The as cast samples of this particular subsystem presented the compositions reported on the last quarterly report. The intended levels of variation for Titanium were 0.5 and 1.5 wt % as presented in table 6.

Table 6. Ternary System: Ni-Ti-Cr

Alloy ID (target)		Ti	Cr
Alloy 27 (Ni-0.5Ti-15Cr)	Minimum	0.72	14.62
	Maximum	0.95	14.98
	Average	0.81	14.74
Alloy 28	Minimum	1.64	14.99

(Ni-1.5Ti-15Cr)	Maximum	1.81	15.76
	Average	1.71	15.38
Alloy 29 (Ni-0.5Ti-20Cr)	Minimum	0.5	20.46
	Maximum	0.48	20.42
	Average	0.58	21.0

In the case of the alloys of the subsystem Ni-Cr-Ti, the alloys showed that the measured transformation temperatures were close together and their mushy zones also were narrow. The effect of increasing the Ti content was decreasing the measured solidus and liquidus temperatures in a magnitude between the stronger effect of Nb and the milder Al effect.

The SEM/EDX analysis of the samples used for DTA experiments showed that the bulk of the samples were practically depleted of Ti after the DTA experiments. Nevertheless, the DTA offset data followed the tendency of the theoretical equilibrium simulations and showing particularly good agreement in the liquidus temperature.

In summary, when the major elements were held constant, the increase in the amount of minor elements like Nb, Ti and Al decreased the transition temperatures, in respectively decreasing extends.

B) Partition Coefficients Determination

The partition coefficients were studied using two different methodologies, by indirect method using DTA experiments followed by pseudo binary system approximation, and by direct measurement using modified DTA experiments (quenching DTA) followed by SEM/EDX analysis.

In the case of indirect measurement, the method was based on DTA experiments on which the solidus and liquidus temperatures were determined for model alloys with varying amount of interest solute element, and drawing the experimental solidus and liquidus trend lines in the corresponding pseudo binary diagram. The ratio of the slopes for the liquidus and solidus constitutes a simple measurement of the partition coefficient of the varying solute element. All partition coefficients determinations were independent of the offset that some subsystems required, because the offset did not affect the slopes of the experimental trend lines.

Usually the change of the partition coefficients with the temperature is related to changes in slope of the liquidus and solidus lines. Synthetic phase diagrams approach has been used [25] where the partition coefficients are considered constant while the curvature of the liquidus and solidus lines are regarded independently. It was found that the error introduced to the calculations of microsegregation, by assuming straight phase boundaries lines is amplified when pseudo binary diagrams are used to approximate multi-element alloys. Therefore, the results for the partition coefficient of the solute elements from the indirect method should be pondered carefully.

a) Partition coefficient of Nb and Cr

The partition coefficient of Niobium was studied for the ternary subsystems Ni-Cr-Nb, Ni-Fe-Nb and for the quaternary subsystem Ni-Cr-Fe-Nb. The influence of the type and amount of major solute elements was taken into consideration.

The results for the indirect measurements for the partition coefficient of Niobium in the Ni-Cr-Nb subsystem are presented in table 7. It was assumed that the solidus and liquidus lines are straight lines not having the same starting temperature at zero Niobium content.

Table 7. Indirect measurements of Nb partition coefficient for Ni-Cr-Nb alloys

Type of alloy	Experimental Solidus trend line	Experimental Liquidus trend line	Experimental K_{Nb} (partition coeff. Nb)	Theoretical K_{Nb} (partition coeff. Nb)
Ni-15Cr-XNb	-10.406x+1429.5	-4.9311x+1438.8	0.4737	0.29 ~ 0.38
Ni-20Cr-XNb	-17.436x+1421	-11.629x+1451.6	0.666	0.54 ~ 0.57

Theoretical simulations were performed using the ThermoCalc software with the equilibrium method and the commercial database. The partition coefficient of Nb was calculated as function of the solid fraction and the minimum and maximum values are included in the table 1 for comparison with the experimental values.

The experimental partition coefficient of Niobium determined by the indirect method was bigger than the theoretically predicted one, for both levels of Chromium. Also, the partition coefficient of Nb increased with the increase in the amount of Chromium, a tendency that was opposed to the one found in all simulations performed using the equilibrium, Scheil and Dictra methods (Fig.10). The partition coefficient of Chromium was determined using the indirect method, for both low and high levels of Niobium. The results are presented in the table 8.

Table 8. Indirect measurements of Cr partition coefficient for Ni-Cr-Nb alloys

Type of alloy	Experimental Solidus trend line	Experimental Liquidus trend line	Experimental K_{Cr} (partition coeff. Cr)	Theoretical K_{Cr} (partition coeff. Cr)
Ni-XCr-3Nb	-2.2103x+1465.9	-1.466x+1472.4	0.66	~
Ni-XCr-6Nb	-7.3722x+1502.2	-6.9343x+1526.6	0.94	~

The direct determination of the partition coefficients of the solute elements was performed by SEM/EDX microprobe analysis of DTA samples quenched from the mushy zone. The random point technique was performed and solute profiles were obtained by studying the gamma primary dendrites.

The collected data set for each alloy was ranked according to the partitioning tendency of the elements and assigned an apparent solid fraction from 0 to the measured solid fraction f_s . The profiles obtained were fitted to the Scheil equation of microsegregation (Equation 1) using the square norm of the error vector (Equation 2).

$$C_s = kC_0(1 - f_s)^{(k-1)} \quad [1]$$

$$Error = (C_s^* - C_s)^2$$

$$Error = (C_s^* - kC_0^*(1 - f_s)^{(k-1)})^2 \quad [2]$$

C_s^* = Measured Solid Composition (dendrite profile)

C_0^* = Measured overall Composition

Fig.25 shows the fitting error vs. the partition coefficient of Niobium in model alloy with low level of Chromium. It can be seen that the value of 0.494 for the partition coefficient of Niobium best fits the experimental data to the Scheil equation. The effect of increasing the amount of Chromium was included by determining the partition coefficient of Niobium with the above described method for the correspondent alloy with high level of Chromium. The fitting error to the Scheil equation was minimized when the partition coefficient of Niobium was 0.67 as shown in Fig 26.

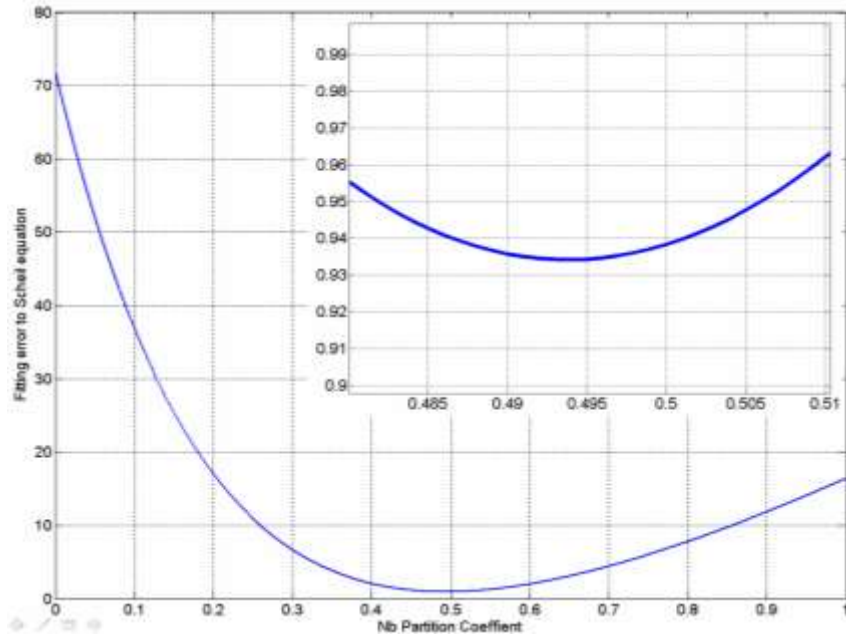


Fig. 25 Fitting error to Scheil equation vs. partition Coefficient of Niobium in alloy Ni-15.4Cr-3Nb.

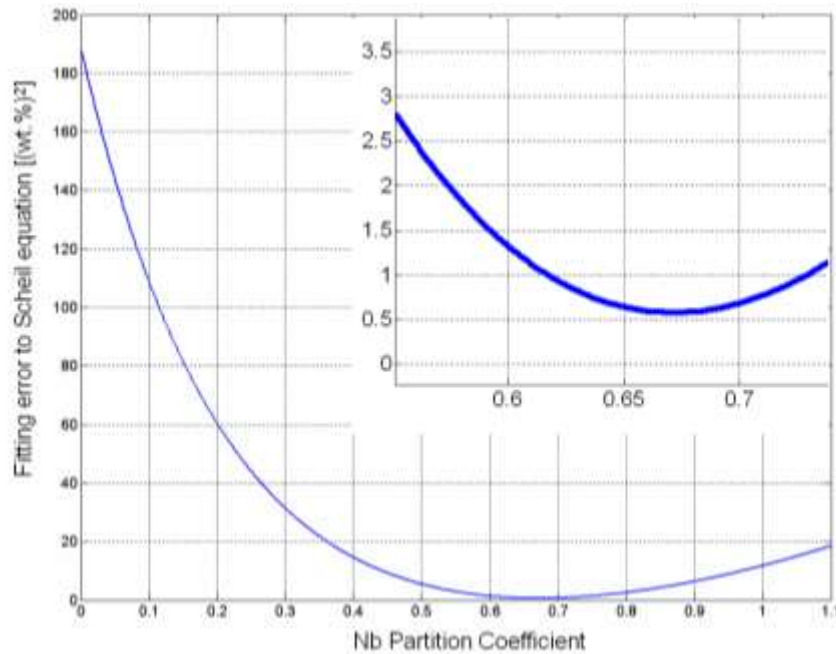


Fig. 26. Fitting error to Scheil equation vs. Partition Coefficient of Niobium in alloy Ni-17.17Cr-3Nb

Following the same methodology, the partition coefficient of Chromium was determined to minimize the fitting error when it takes the value of 1.0, as shown in the Figure 27, which corresponds to the model alloy Ni-17.17Cr-3Nb.

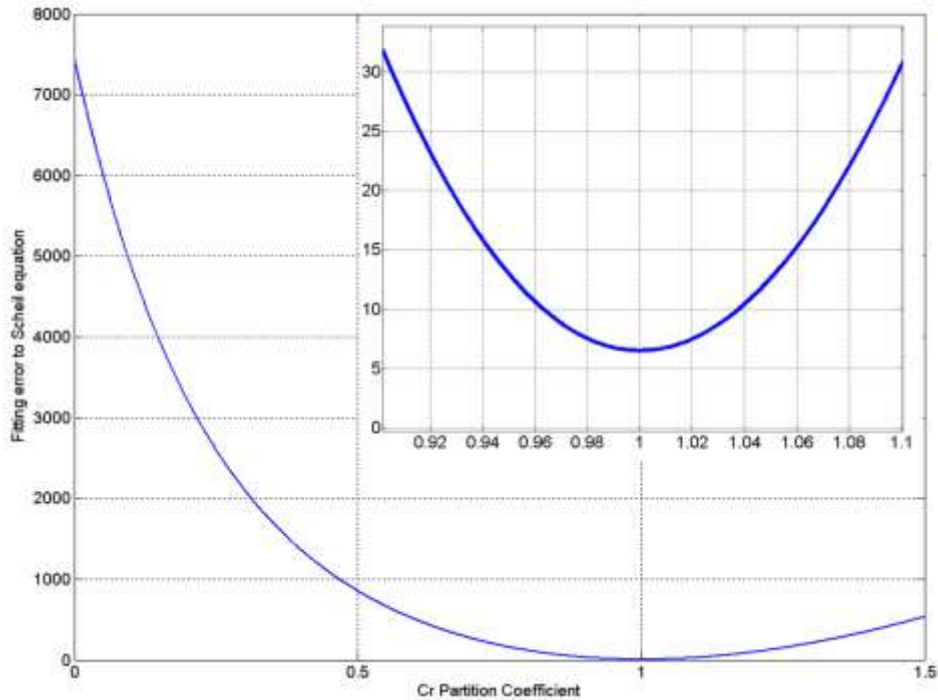


Fig. 27 Fitting error to Scheil equation vs. Partition Coefficient of Chromium in alloy Ni-17.17Cr-3Nb

The experiments with the model samples of the system Ni-Cr-Ti showed that the Partition coefficient of Chromium decreased to a value of 0.8 when the content of Titanium was 1.5 Wt.%

b) Partition coefficient of Fe

Partition coefficient of Fe for the subsystem Ni-Fe-Nb was determined by modified DTA technique combined with the measured profile fitting described previously.

The partition coefficient of Fe was found to be 1.045 as observed in Fig. 28. The presence of Fe as major alloying element decreased strongly the partition coefficient of Nb, to an approximate value of 0.16. Fig. 29 shows the fitting error to Scheil equation and the value of K_{Nb} that minimizes its magnitude.

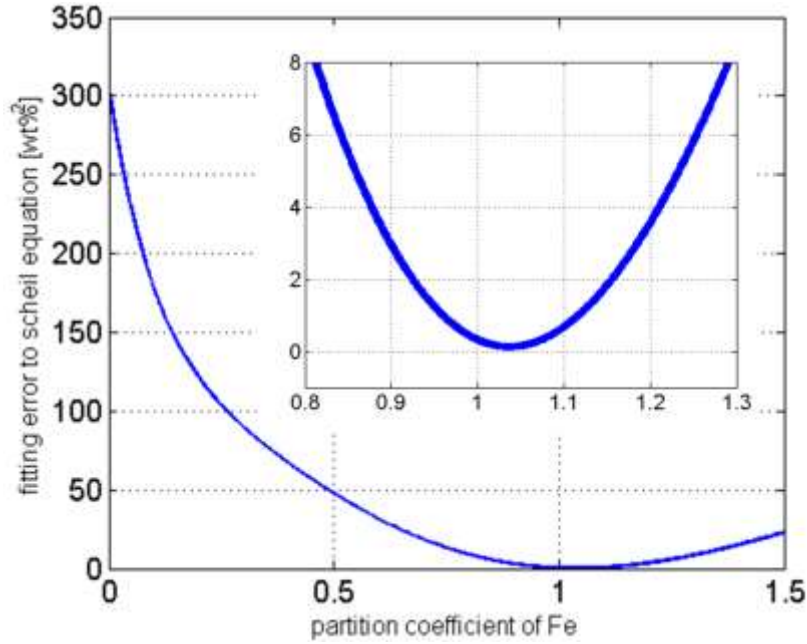


Fig. 28 Fitting error to Scheil equation vs. Partition Coefficient of Fe in alloy Ni-5Fe-3Nb

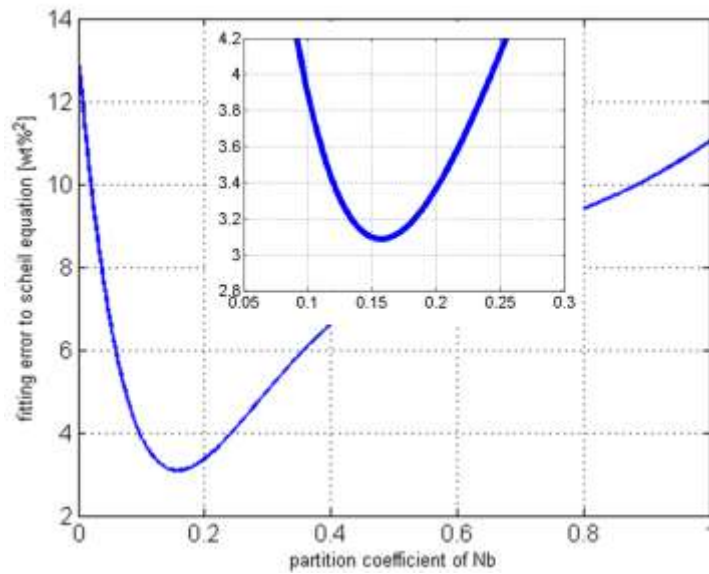


Fig. 29 Fitting error to Scheil equation vs. Partition Coefficient of Nb in alloy Ni-5Fe--3Nb

During the SEM/EDX analysis, the quenched model sample of alloy 7, which had an average as cast composition of Ni-3.88Nb-5.28Fe presented a microstructure composed of primary dendrites and an eutectic like interdendritic material composed of dendrites with a secondary phase found to have a composition of about 50 At%Ni, 50At%Nb matching with great approximation to the equilibrium phase Ni_6Nb_7

c) Partition Coefficient of Al

The direct measurement technique was used to determine the partition coefficient of Al in the subsystem Ni-Cr-Al.

The partition coefficient of Al was found to be slightly greater than one, meaning that the Aluminum redistributes preferentially in the primary dendrites rather than in the interdendritic liquid, as shown in the fig. 30 where the value of the partition coefficient that minimizes the error is approximately 1.21

The same methodology was used to determine the partition coefficient of Chromium and its value was 1.08.

The interaction between the minor elements Nb and Al was evaluated for the quaternary alloy Ni-20Cr-4.9Al-6Nb and the resulting partition coefficients are presented in table 9.

The presence of Aluminum increased the partition coefficient of Niobium reducing its microsegregation to the interdendritic liquid.

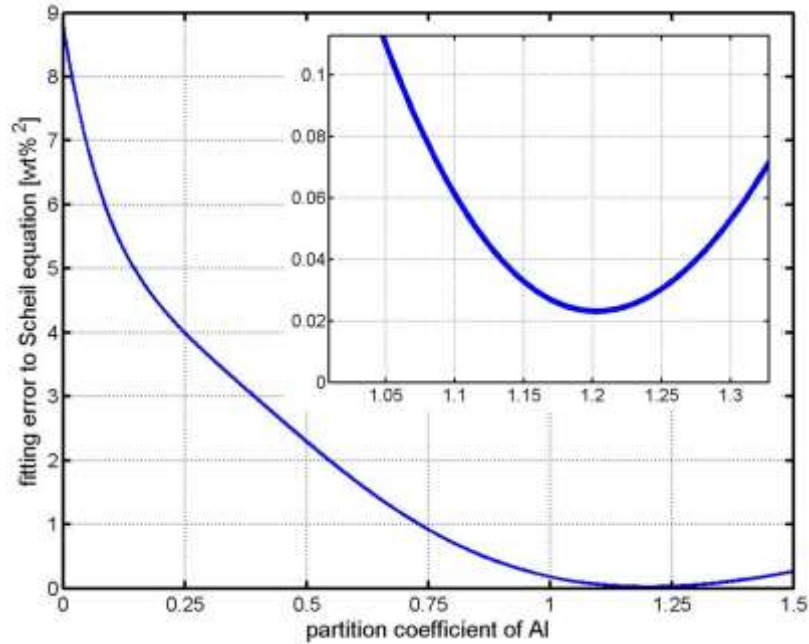


Fig. 30 Fitting error to Scheil equation vs. Partition Coefficient of Aluminum in alloy Ni-20Cr-4.9 Al-6Nb

Table 9. Measured partition coefficients by profile fitting

K_{Nb}	K_{Cr}	K_{Al}
0.785	1.02	1.11

d) Partition Coefficient of Ti

The MDTA experiments were performed for all the alloys of the Ni-Cr-Ti subsystem, following the same methodology previously described. On the SEM/EDX examination of the samples, it was observed that the amount of Titanium on the bulk of the samples was highly reduced, while a continuous layer of oxide with high content of Ti was found in all processed samples.

Although the data collected was not suitable to determine the partition coefficient of Ti by the direct measurement, its influence on Chromium partition coefficient was evident and the result for Alloy 28 is showed in Fig. 31. Currently, modifications of the procedure of MDTA experiments are being proposed in order to prevent the depletion of Titanium observed.

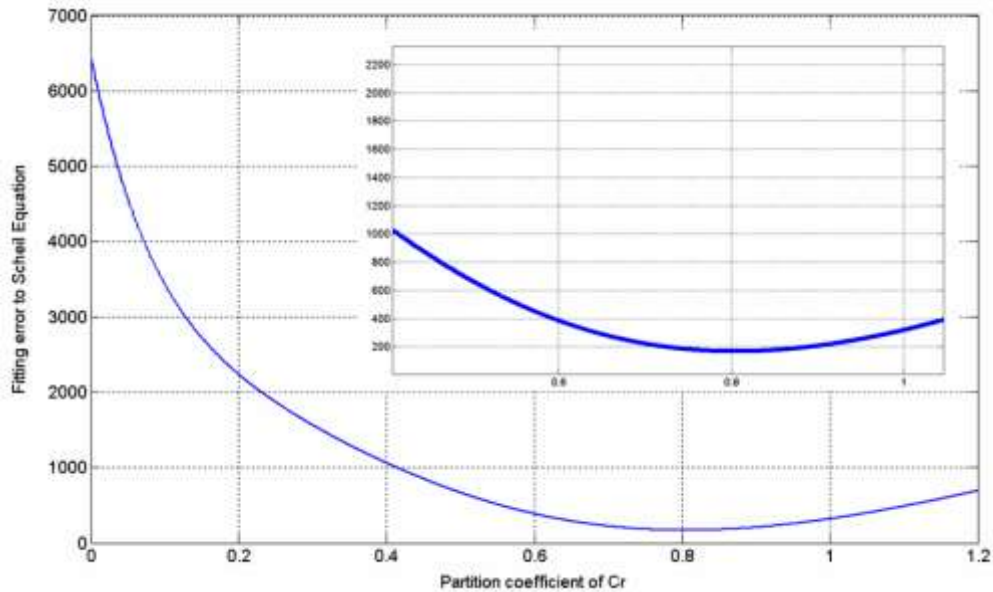


Fig.31 Partition Coefficient of Chromium for Alloy 28: Ni-1.5Ti-15Cr

Sub-task 1.1.3 Kinetic Effects

There is a wide agreement in the concept that it is more probable to induce undercooling to DTA samples from the liquid state during the solidification reaction than superheating the solid samples during the melting stage of the experiment [26].

In this investigation, the kinetic effect did not manifested equally for all the subsystems studied. In the case of the subsystem Ni-Cr-Nb, an increase of the heating and cooling rates of about three times the original value (from 3 °C/ min to 10 C/min) did not induced noticeable effects on the phase transformation reactions as can be observed in Fig. 32

Meanwhile, the subsystem Ni-Fe-Nb was found to be the most sensitive to the kinetic effects. In Fig. 33 can be observed that an increase from 5 °C/ min (bottom) to 10 °C/ min (top) in the cooling rate induced a lowering shift of the solidification reaction of about 100 °C.

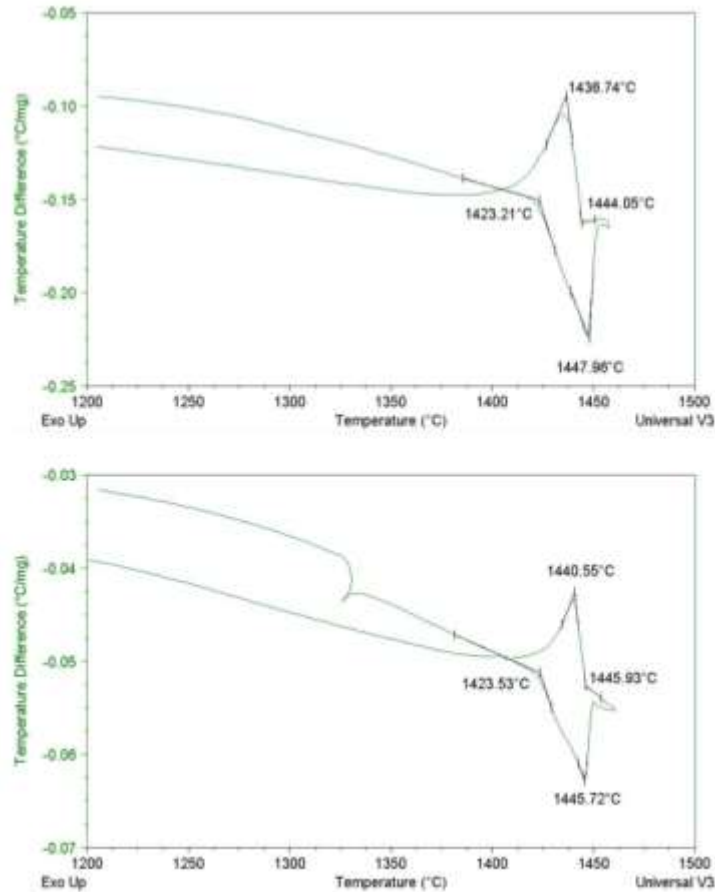


Fig. 32 DTA curves for alloy 2 at 10 °C/ min (top) and 3°C/ min (bottom)

The quaternary subsystem Ni-Cr-Fe-Nb was included in the regular DTA experiments and the heating /cooling rates were fixed to 25 °C/ min for all the experiments performed for the set. The experimental results showed that the experimental liquidus temperatures were in great agreement with the theoretical simulations, while the solidus temperature was always registered above the predicted values. In addition, the variability of the solidus data was greater and the CVI was almost homogeneous for all the corresponding model alloys.

The modified DTA experiments were performed according to the proposed experimental plan. The samples were cooled from the liquid state at a fixed rate until reaching the mushy zone range, and then the quenching step was executed. Improvements were required for the modified thermocouple assembly design in order to facilitate the recognition of the phase transformation points in the MDTA curves generated.

During the quenching experiments and the later analysis performed by optical and electron microscopy it was found that the quenched samples presented a microstructure composed of primary gamma dendrites and interdendritic quenched liquid which transformed to secondary (tertiary) dendrites and fine eutectic structure. Regarding the cooling rate imposed in the MDTA experiments, the eutectic reaction was not suppressed and makes it acceptable to suppose that near local equilibrium state was maintained at the interface solid-liquid during the solidification in the quenching oil pool, i.e. there was no significant supercooling of the dendrites tips, and the nonequilibrium lever rule was still applicable [27], [28], giving reliability to the partition

coefficients obtained from fitting the segregation profiles found on the primary gamma dendrites to the Scheil model.

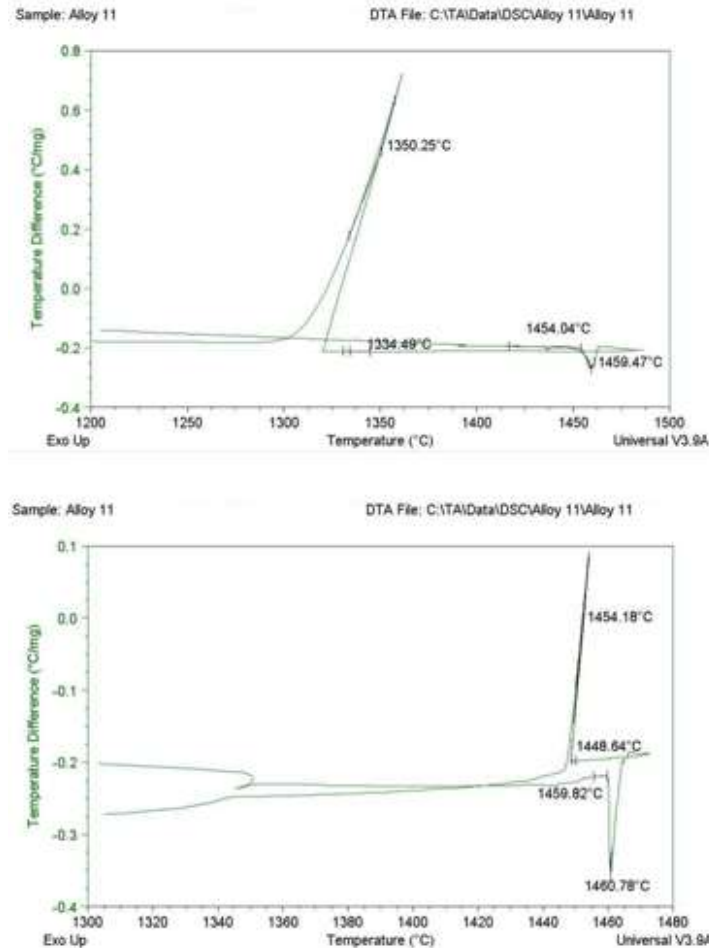


Fig. 33 DTA curves for alloy 11 at 10 °C/ min (top) and 5 °C/ min (bottom)

Task 1.2 Solidification Modeling

In this subtask the partition coefficients obtained from the DTA and MDTA experiments were substituted into the WVU model. The relative Rayleigh number developed by WVU researchers was updated and differences were pointed out with respect to the expected magnitude of the Rayleigh number for the model alloys.

The relative Rayleigh number (Ra^*) derived in WVU for application in Industry, where the production conditions and geometric parameters are practically constant, considers only the compositional effect on the freckling tendency.

$$Ra^* = \frac{\Delta\rho \cdot \Pi}{f_i} \quad [3]$$

When $\Delta\rho$ is the density change $((\rho - \rho_0)/\rho_0)$, Π is the permeability of the mushy zone in the direction perpendicular to the primary dendrite arms and f_l is the liquid fraction.

CALPHAD Approach: The solute profiles (liquid composition) are obtained by Dictra at the cooling rates established. With the profiles, the dependence of chemical composition of the interdendritic liquid with temperature can be determined. The chemical composition vs. temperature can then be used to determine the dependence of density with temperature. The density change of the interdendritic liquid then is used to calculate the Rayleigh number.

Experimental Approach: The solute profiles are measured by random point SEM/EDS analysis for the samples of DTA experiments at the respective cooling rates. The chemical composition change of the interdendritic liquid is translated to density change with temperature and the Rayleigh number is calculated by semi-empirical methodology.

The calculation of the relative Rayleigh number for model alloys started using the already collected SEM/EDS data for samples corresponding to the subsystem Ni-Cr-Nb. With the solute profiles determined experimentally, the change of density of the interdendritic liquid was calculated using the methodology of the additive molar fraction on which the density of the liquid is calculated by:

$$\rho = \frac{\sum_i x_i A_i}{\sum_i x_i V_i} \quad [4]$$

Where ρ is the density of the liquid alloy at the temperature of analysis (i.e. at the corresponding liquid fraction), while x_i , A_i , V_i are the molar fraction, the atomic weight, and the molar volume of i^{th} element respectively. No mixing factor was included due to the fact that it becomes negligible for the model alloys studied in this work. The permeability was determined by the expression developed by Poirier and improved by W. Yang et al [29] for interdendritic flow perpendicular to the primary dendrite arms:

$$\Pi = \frac{\Delta T}{\int_0^{\Delta T} f_L^{-3.34} \cdot dT} \quad [5]$$

Fig.34 shows the results for the Relative Rayleigh Number calculated for model alloy 1 and model alloy 4, which were Ni-15Cr-3Nb and Ni-20Cr-3Nb respectively. The maximum value is located approximately at 0.5 fraction liquid for both alloys. Alloy 4 shows a higher maximum relative Rayleigh number, so it is expected that for the same cooling conditions and geometry, this alloy will have a higher tendency for macrosegregation than Alloy 1.

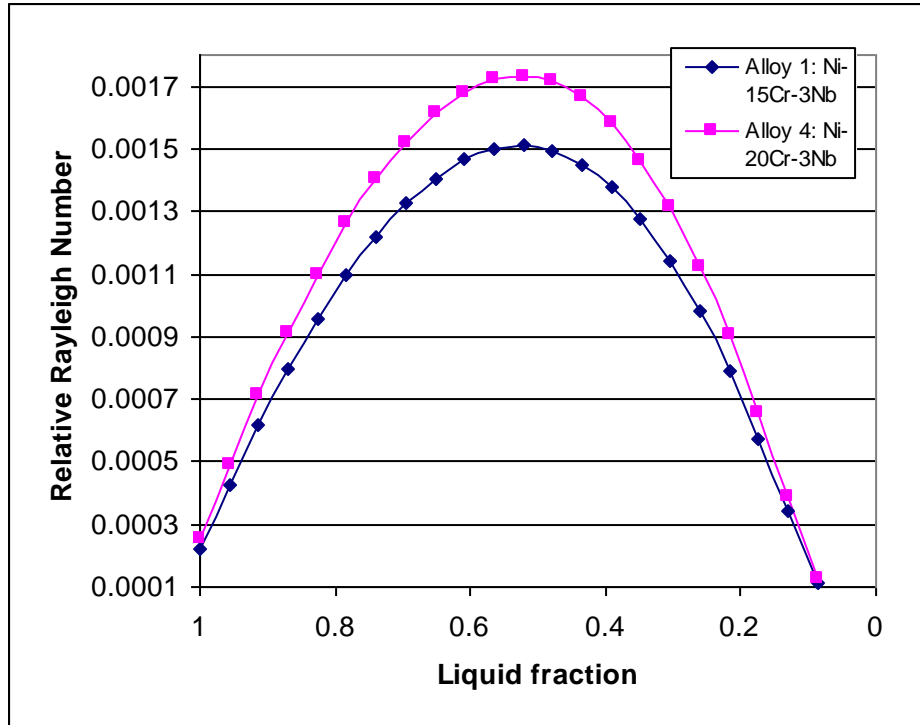


Fig.34 Relative Rayleigh Number for Alloy 1 and Alloy 4.

The Rayleigh Number was calculated using the expression derived by the WVU researchers from the Flemings criterion, with the form:

$$Ra = \frac{\Delta\rho \cdot g \cdot \Pi}{\nu \cdot f_L} \cdot \frac{1}{R} \quad [6]$$

Where $\Delta\rho$ is the density change ($(\rho - \rho_0)/\rho_0$), g is gravity, Π is the permeability, ν is the viscosity of the interdendritic fluid, f_L is the averaged fraction liquid in the mushy zone, and R is the crystal growth rate.

The permeability can be calculated by equation 5. It is known that the crystal growth in the mushy zone can be defined by the expression:

$$\varepsilon = -G \cdot R \quad [7]$$

Where G is the thermal gradient and ε is the cooling rate. The negative sign indicates that the gradient and the crystal growth have opposite directions. With the measurement of the gradient and the cooling rate, the crystal growth rate could be derived. From the exploration experiments using the DS furnace, the gradient was found to be 7.38 °C/cm.

The cooling rates will be fixed according to the experimental plan proposed below in task 2.1.

For the same chemical composition (alloy 1), the influence of the cooling rate was observed on the Rayleigh number. The increase of the cooling rate from the low level (3 C/min) to the high level (9 C/min) decreased the maximum Rayleigh in more than 50 %.

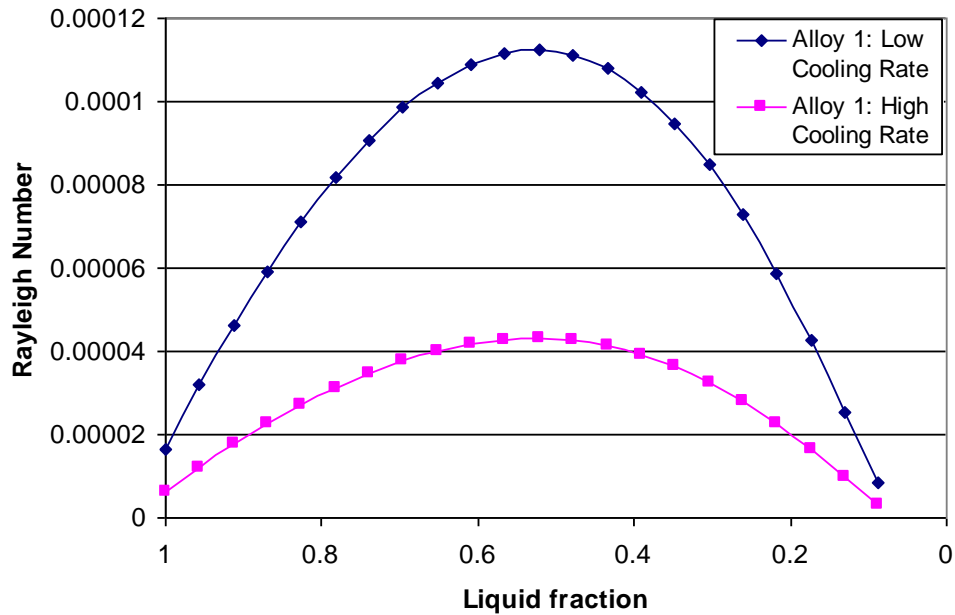


Fig. 35 Rayleigh Number for Alloy 1 at low cooling rate and high cooling rate

Task 2 Directional Solidification Verification

The model alloys were selected aiming to study the effects of composition and the type of eutectic reaction, on the freckling tendency. Currently, modifications on the Rayleigh Number definition are being proposed and the following aspects are taken into account:

- Considering the effect of the slope of the mushy zone in the definition of the characteristic length, and confront with freckle criterion on tilted solidification front proposed by Wang-Hong Yang et al [30]
- Improve the approximation for the integration in the permeability definition on equation 5.
- The omission of the mixing factor for the model alloys because its magnitude becomes negligible for the solute elements involved.
- Include recent advances in the theoretical description of flow in anisotropic porous media

A catastrophic failure was reported in the ceramic retort tube of the Directional Solidification furnace that delayed the development of this task and subsequently, the verification on model alloys corresponding to the task 2.1 and the verification for commercial alloys in task 3.

Task 2.1 Verification of Model Alloys (Liu/WVU)

Experiments of horizontal directional solidification will be performed with the intention of comparing the freckling predictions by Rayleigh number criterion developed using CALPHAD methodology and by experimentation.

Differences between the freckling predictions will be useful to understand and point out the limitations of the predictions based on the commercial databases developed for the Ni-base superalloys.

Selected model alloys will be melted and horizontally solidified under controlled directional solidification conditions at rates that are known to be critical for macrosegregation. Previous experiments showed that alloys similar to the ones proposed, showed freckles during directional solidification, and the summary of the results is shown in Table 10 [31].

Table 10. Freckling Cooling rates in Model Alloys

Model Alloys studied	Cooling Rate at the position of initiation of freckle
RN902 (Ni-19.95Cr-17.76Fe-7.13Nb)	8.5 °C /min
RN903 (Ni-20Cr-8.6Nb)	2 °C/min
RN904 (Ni-20.17Cr-5.7Ti)	0.6 °C/min

a) Selection of the Model alloys for DS experiments

Nb Content:

The chemical composition is selected to facilitate the freckles formation. The amount of Nb will be selected as high as possible because the freckling potential is higher at the solubility limit of Nb in proeutectic gamma phase, but to maintain similarity with commercial alloys, Nb content will be 6 Wt.%

The amount of Chromium will be selected at 20 Wt.% The theoretical calculations predicted that the increase in Chromium content lowered the magnitude of the Nb partition coefficient, implying that its segregation will be higher, while the experimental results suggested that the Nb partition coefficient increases with increasing amount of Cr. The Directional Solidification experiments will serve to study in more depth this inconsistency.

The selected model alloys of the ternary system Ni-Cr-Nb are:

Ni-20Cr-6Nb : Model Alloy 6 (DS1)

Ni-15Cr-6Nb : Model Alloy 3 (DS2)

Al Content:

W. Yang et al. (1999) measured the Aluminum initial partition coefficient to be 1.05 and in this work it's value was found to be between 1.11 and 1.21. Being the Aluminum a lighter element, its preferential partition to the solid makes the interdendritic liquid heavier than the bulk liquid, adding a freckling tendency to the segregation of heavy Niobium. Considering this, the aluminum will be selected in the high level studied in the model alloys, that is 1.0 Wt %.

Ni-20Cr-1.0Al: Model Alloy 22 (DS3)

Ti content:

The partition coefficient of Ti was measured in commercial alloy IN-718 by Wanhong Yang et al. and found its magnitude to be approximately 0.59. The microsegregation of Ti makes the interdendritic liquid lighter, and freckle formation in Ti-containing alloys was observed for model alloys under horizontal directional solidification.

The model alloy selected will have the higher level of Titanium studied on the DTA experiments.

Ni-20Cr-1.5Ti: (DS4)

b) Directional Solidification furnace capabilities

The directional solidification furnace consists of a cylindrical retort alumina tube, closed in one end and isolated in the radial direction. The furnace is heated up by the use of 6 heating elements located in two rows, each side of the retort alumina tube. The heating units are made of molybdenum disilicide, which can withstand a maximum temperature of 1700 °C.

The design of the furnace permits controlling the temperature in three different zones independently, giving the option to fix the temperatures in those three points along the longitudinal direction.

The heat flux is unidirectional and is induced in the open end of the retort tube by means of a water cooling system.

During the calculation of the relative Rayleigh number for the model alloys, the commercial alloy IN-718 was included, according to the composition on the corresponding data sheet reported by SMC [32]. Fig. 36 shows the Relative Rayleigh Number variation with Liquid Fraction for alloy IN-718.

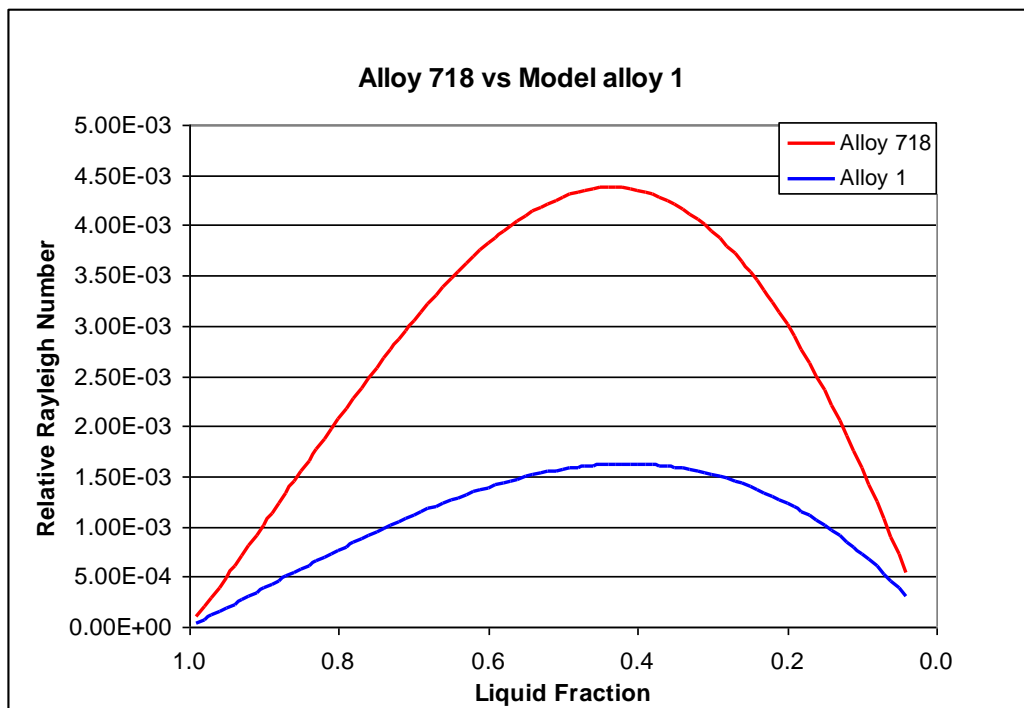


Fig. 36 Relative Rayleigh number for Alloy IN-718

When compared with the model alloy 1, the commercial alloy IN-718 showed a higher relative Rayleigh Number at about 0.6 Solid Fraction.

Task 2.2 Effect of Processing Parameters

Experimental Plan

The experimental plan includes two parameters or control variables, which are the chemical composition of the alloys and the cooling rate. The chemical composition will vary within four different levels as defined above, while the cooling rate will vary between two levels. Hence, eight different configurations for directional solidification experiments will be included.

Preliminary exploration runs should be performed to fine tune the heating/cooling cycles for each zone of the furnace, to attain the cooling rates throughout the molten liquid. At least three repetitions of the definitive experiments are expected to be performed for each of the eight different configurations presented in Table 11. The experimental design will consider the existence of freckles as response variable (output variable).

Table 11. Configuration of Variables for DS experiments

	Cooling Rate: low level	Cooling Rate: high level
COMPOSITION	3 C/min	9 C/min
DS1:a	ar	aR
DS2:b	br	bR
DS3:c	cr	cR
DS4:d	dr	dR

The exploration runs will be developed using the same crucibles and sample size that will be used in the definitive experiments.

The design of the furnace permits that the heat flux occurs in the longitudinal direction, and being the heat transfer unidirectional, the distribution of temperatures along the axis can be calculated analytically.

The control system of the furnace will permit defining three points along the axis with almost constant temperatures, but changing heat flux in time. The tray crucibles were selected of a length that permits to locate them with the constant temperature points coinciding with the ends, so creating a gradient over the molten metal that can be easier to control.

To support the exploration runs set up, finite elements simulations of the heat transfer phenomenon will be developed and validated with analytical method. The data collected will feedback the process of fine tuning.

Task 3: Verification for Commercial Alloys (WVU/SMC/GE Energy)

The verification on commercial alloys will be performed once the Directional Solidification furnace is brought back to functional condition. Currently, the specially designed crucibles are being expected to be delivered, while improvements of the equipment were proposed and developed to enhance the capability of the data storage and posterior analysis.

The set point temperature dependence with time for each of the heating zones of the directional solidification furnace will be defined. The corresponding control curves will induce thermal conditions during solidification that will permit selecting the cooling rate, the thermal gradient and the isotherm speed through the molten metal inside the crucible.

The crucibles to be used have a parallelepiped shape, which facilitates the conditions of planar solidification front. Besides, the bases of the crucibles have a smaller area compared to the top surfaces, to permit easier extraction of the solidified samples.

The experiments proposed for task 2 include the most important compositions according to the results of this work, and cover the alloys recommended on a previous project developed by WVU researchers [31]. The results for the DS experiments will serve to evaluate the influence of the factors or processing parameters over the response variable and the observed tendencies will be confirmed for commercial alloys. A more accurate criterion is expected to be developed for the freckling tendency in the VAR ingots, based on the Rayleigh number conceptual frame. The refined solidification model will then be used to analyze the available Industrial data. The verification for Commercial alloys will follow a Design of experiments similar to the one proposed on task 2.2. Finally, a ranking of macro segregation tendency will be prepared from the results of Directional Solidification experiments, including both, the selected model and commercial alloys.

Plan for the future:

Task 1: Solidification Modeling

Task 1.1 Thermodynamics Database and Partition Coefficients

Sub-task 1.1.1 Thermodynamic Modeling (Liu/PSU)

In the future the following tasks will be performed for this project:

- (i) to submit the first paper within one or two months: Partition behaviors of alloying elements in the Ni-Cr-Nb alloys: thermodynamic and kinetic investigations
- (ii) to finish the thermodynamic modeling in the Ni-Fe-Nb system and publish it.
- (iii) to finish the thermodynamic modeling in the Cr-Fe-Nb system and publish it.

Sub-task 1.1.2 Experimental Investigation on Partition Coefficients (Liu/WVU)

In the future the following tasks will be performed for this project:

- (iv) to perform DTA experiments for the quaternary subsystems not included so far
- (v) to perform MDTA experiments for repetitions of the model alloys of the subsystem Cr-Ni-Ti

[1] Du Y, Liu SH, Chang YA, Yang Y. Calphad-Computer Coupling of Phase Diagrams and Thermochemistry 2005;29:140.

[2] Tomiska J. J Alloy Compd 2004;379:176.

[3] Raghavan V. Journal of Phase Equilibria and Diffusion 2004;25:552.

[4] Cacciamani G, De Keyzer J, Ferro R, Klotz UE, Lacaze J, Wollants P. Intermetallics 2006;14:1312.

[5] Raghavan V. Journal of Phase Equilibria and Diffusion 2004;25:554.

[6] Saunders N, Miodownik AP. CALPHAD (Calculation of Phase Diagrams): A Comprehensive Guide 1998.

[7] Joubert JM, Feutelais Y. Calphad-Computer Coupling of Phase Diagrams and Thermochemistry 2002;26:427.

[8] Tewari SN. Metallography 1980;13:379.

-
- [9] Chen HL, Du Y. Calphad-Computer Coupling of Phase Diagrams and Thermochemistry 2006;30:308.
- [10] Toffolon C, Servant C. Calphad-Computer Coupling of Phase Diagrams and Thermochemistry 2000;24:97.
- [11] Takeyama M, S. Morita, A. Yamauchi, M. Yamanaka, Matsuo T. Superalloys 718, 625, 706 and Various Derivatives, E.A. Loria, Ed., The Minerals, Metals and Materials Society 2001:333.
- [12] Savin VV. Fizika Metallov I Metallovedenie 1989;68:143.
- [13] Andersson JO, Helander T, Hoglund LH, Shi PF, Sundman B. Calphad-Computer Coupling of Phase Diagrams and Thermochemistry 2002;26:273.
- [14] Campbell CE, Boettinger WJ, Kattner UR. Acta Mater 2002;50:775.
- [15] Saunders N, Fahrman M, Small CJ, editors, Green KA, Pollock TM, Kissinger RD. TMS, Warrendale, PA 2000:803.
- [16] Lee BJ. Calphad-Computer Coupling of Phase Diagrams and Thermochemistry 1992;16:121.
- [17] Bratberg J, Frisk K. Metallurgical and Materials Transactions a-Physical Metallurgy and Materials Science 2004;35A:3649.
- [18] Zunger A, Wei SH, Ferreira LG, Bernard JE. Phys. Rev. Lett. 1990;65:353.
- [19] Wei SH, Ferreira LG, Bernard JE, Zunger A. Physical Review B 1990;42:9622.
- [20] Jiang C, Wolverton C, Sofo J, Chen LQ, Liu ZK. Physical Review B 2004;69:214202.
- [21] Shin D, Arroyave R, Liu ZK, Van de Walle A. Physical Review B 2006;74:024204.
- [22] Shin D. *Ph. D. thesis*. University Park: Pennsylvania State University; 2006.
- [23] S. Shang, Z. Liu, Presentation for STAC meeting, WVU, Morgantown, WV, 2006
- [24] F. Zhang, S. Lien, W. Cao, Y. Sang, K. Wu, Y.A. Chang, Application of Phase Diagram Calculation for Aerospace Materials: in Aeromat , Baltimore, MD, 2007.
- [25] www.calphad.com/nickel-chromium.html
- [25] M. Rettenmayr , T. Kraft : Metall. Trans. A, 1997, Vol.28A, pp.447-451
- [26] Q. Feng, L.J. Carrol, and T.M. Pollock, Metallurgical and Materials Transactions , 37A (2006) 1949-1962
- [27] J. Sarreal , G. Abbaschian,; Metall. Trans. A, 1986, Vol. 17A, pp. 2063-2073
- [28] M.C. Flemings: Solidification Processing, McGraw-Hill, New York, 1974, pp.34-36.
- [29] W. Yang, W. Chen, K-M. Chang, S. Mannan, J. J. deBarbadillo, Freckling Criteria for the Upward Directional Solidification, Met. Trans. A., (32A) 2001, pp.397-406
- [30] Wang-Hong Yang, John J. deBarbadillo, Kori Morita, T. Suzuki, Wei Chen, Keh-Minn Chang, A freckle criterion for the Solidification of Superalloys with a tilted Solidification Front, JOM, September 2004, pp. 56-61
- [31] Keh-Minn Chang, Horizontal Solidification of Nickel-Based Model Alloys, WVU, 2000. Report for Daido Steel Company
- [32] <http://www.specialmetals.com/documents/Inconel%20alloy%20718.pdf>